Acta Pharmaceutica Sinica B 2024;14(6):2520–2536

Chinese Pharmaceutical Association
Institute of Materia Medica, Chinese Academy of Medical Sciences

Acta Pharmaceutica Sinica B

www.elsevier.com/locate/apsb
www.sciencedirect.com

ORIGINAL ARTICLE

Interferon-induced MXB protein restricts vimentin-dependent viral infection

Dongrong Yi[a,†], Ni An[a,†], Quanjie Li[a,†], Qian Liu[a,†], Huihan Shao[a], Rui Zhou[a], Jing Wang[a], Yongxin Zhang[a], Ling Ma[a], Fei Guo[b], Xiaoyu Li[a], Zhenlong Liu[c,*], Shan Cen[a,*]

[a]*Institute of Medicinal Biotechnology, Chinese Academy of Medical Science, Beijing 100050, China*
[b]*Institute of Pathogen Biology, Chinese Academy of Medical Science, Beijing 100730, China*
[c]*Lady Davis Institute for Medical Research, Jewish General Hospital, Montreal, Quebec H3T 1E2, Canada*

Received 7 December 2023; received in revised form 16 February 2024; accepted 14 March 2024

KEY WORDS

MXB;
Vimentin;
Broad antiviral strategy;
Cytoskeleton network;
AKT

Abstract Type I interferon (IFN) inhibits a wide spectrum of viruses through stimulating the expression of antiviral proteins. As an IFN-induced protein, myxovirus resistance B (MXB) protein was reported to inhibit multiple highly pathogenic human viruses. It remains to be determined whether MXB employs a common mechanism to restrict different viruses. Here, we find that IFN alters the subcellular localization of hundreds of host proteins, and this IFN effect is partially lost upon MXB depletion. The results of our mechanistic study reveal that MXB recognizes vimentin (VIM) and recruits protein kinase B (AKT) to phosphorylate VIM at amino acid S38, which leads to reorganization of the VIM network and impairment of intracellular trafficking of virus protein complexes, hence causing a restriction of virus infection. These results highlight a new function of MXB in modulating VIM-mediated trafficking, which may lead towards a novel broad-spectrum antiviral strategy to control a large group of viruses that depend on VIM for successful replication.

*Corresponding authors.
E-mail addresses: shancen@imb.pumc.edu.cn (Shan Cen), zhenlong.liu@mail.mcgill.ca (Zhenlong Liu).
[†]These authors made equal contributions to this work.
Peer review under the responsibility of Chinese Pharmaceutical Association and Institute of Materia Medica, Chinese Academy of Medical Sciences.

https://doi.org/10.1016/j.apsb.2024.03.029

1. Introduction

IFNs provide one key antiviral mechanism in host innate immune response to virus infections by inducing the expression of a cascade of genes collectively called IFN-stimulated genes (ISGs), many of which were previously reported to inhibit diverse viruses[1−3]. Viruses are intracellular pathogens that rely on cellular machineries for their replication[4−6]. Following entry either from the plasma membrane or intracellular membranes including endosomes and lysosomes, viral genome complex frequently needs to traffic along cytoskeletal filaments to reach the right subcellular location, such as endoplasmic reticulum (ER) and the nucleus for replication[7−9]. For example, hepatitis C virus (HCV) and Zika virus rely upon host trafficking machinery to direct their structural proteins and genomes to ER for replication, assembly, and budding[10,11]. Human immunodeficiency virus type 1 (HIV-1), influenza viruses, and most DNA viruses transport the incoming viral nucleocapsids into the nucleus to replicate viral genomes and transcribe viral genes[12−14]. The cytoskeleton network consists of intermediate filaments (IFs), actin filaments, and microtubules which closely communicate with one another[15,16]. In contrast to actin filaments and microtubules which display the structural polarity[17,18], IFs are nonpolar structures providing a flexible scaffold to support signal transduction and vesicular trafficking[19−21]. In particular, VIM filaments, which belong to IFs, were reported to participate in many stages of virus infection, including virus entry, replication, and egress[22,23]. For instance, depletion or structure change of VIM significantly impairs HIV-1 infection[24]. Moreover, VIM regulates translocation of influenza A virus ribonucleoproteins through interacting with it by the binding of the PB2[25]. In addition, VIM also serves as scaffold to recruit viral protein to form a perinuclear viral factory region[22]. For flavivirus, VIM interacts with the dengue virus nonstructural protein 1 or 4A and surrounds Zika envelope protein, both of which contribute to the formation of viral factory and replication of flavivirus[26,27]. However, although numerous studies investigated the interplay between the cellular cytoskeleton network and virus intracellular trafficking, it remains largely unknown whether and, if so, how IFNs and ISGs modulate the cytoskeleton network, which may serve as a broad antiviral mechanism.

Mx proteins, interferon-induced dynamin GTPases, were reported to inhibit viruses of diverse families[28−30]. Human MxA and MXB proteins share very similar domain structures, including the globular GTPase domain and the stalk domain that are connected by the bundle signaling element[31−35]. MXB bears a short N-terminal sequence that is not shared with MXA, which determines its distinct antiviral spectrum[36−38]. Previous research demonstrated that the 91 N-terminal amino acids of MXB confer full anti-HIV and anti-IAV activities when transferred to the N terminus of MXA[39,40]. One common feature of the MXA and MXB antiviral action is impeding the intracellular transport of viral genome and proteins. For example, MXA impairs the transport of the nucleocapsid protein of bunyaviruses to the Golgi compartment and prevents the incoming nucleocapsids of Thogoto virus from being transported into the nucleus[41,42]. MXB deters the nuclear import of HIV-1 DNA and the DNA of herpes simplex virus 1 (HSV-1)[43−45]. The complicated interactions of nucleoporins (NUPs) or nucleoporin-like proteins (such as NUP214 and transport receptor transportin-1), HIV-1 capsid (CA) tubes, CA binding cofactors (such as cyclosporin A (CYPA)), and N-terminus of MXB were previously found to play functional roles in MXB-mediated inhibition of nuclear import of HIV-1 DNA[46]. In a recent study, Malim et al. reported that serine phosphorylation of the N terminus impedes MXB-mediated inhibition of nuclear import of cellular karyophilic cargo[47]. We also found that MXB abrogates HCV nonstructural protein 5A (NS5A) interaction with replication cofactor (CYPA) and its localization to ER[10]. Collectively, the antiviral specificity of MX proteins is achieved by their recognition of viral proteins or host proteins. However, to date, little is known about how MX proteins interfere with the intracellular trafficking of viral protein complexes. In this study, we observed that MXB recruits the AKT kinase to phosphorylate VIM at amino acid S38 and, as a result, causes a reorganization of VIM network and the impaired trafficking and replication of HIV-1 and HCV.

2. Materials and methods

2.1. Plasmid DNA

Full-length MXB cDNA and the cDNA fragment encoding MXB (26−715), MXB (1−334), and MXB (335−715) were cloned into the pcDNA4/TO expression vector (Invitrogen) using the BamHI and NotI restriction sites, with Flag tag labeling to the C termini of proteins. The MXB-GFP and MXB (26−715)-GFP DNA were constructed with the green fluorescent protein sequences adding to the C-terminus of MXB protein. Full-length VIM cDNA was cloned into the pcDNA4/TO expression vector with hemagglutinin (HA) tag attached to the C terminus. Flag-tagged NS5A sequence of HCV was cloned into pcDNA4/TO. NS5A mutations (D316E and Y317N) were generated using a site-directed mutagenesis kit (SBS). MXB small guide RNAs (sgRNAs), 5′-CAC CGT GTG GTG GCA CTG TGC CGA A-3′ (sgMXB-1) and 5′-AAA CTT CGG CAC AGT GCC ACC ACA C-3′ (sgMXB-2), were cloned into lentiCRISPR(v2) to create MXB knockout (KO) cell lines. VIM sgRNAs, 5′-CAC CGT TGC TGA CGT ACG TCA CGC A-3′ (sgVIM-1) and 5′-AAA CTG CGT GAC GTA CGT CAG CAA C-3′ (sgVIM-2), were cloned into lentiCRISPR(v2) to create VIM-KO cell lines. CYPA sgRNAs, 5′-CAC CGG CGT CTC CTT TGA GGT CGG G-3′ (sgCYPA-1) and 5′-AAA CCC CGA CCT CAA AGG AGA CGC C-3′ (sgCYPA-2), were cloned into lentiCRISPR(v2) to create CYPA-KO cell lines. VIM point mutations (S38E, S38A, S83A) were generated by using a site-directed mutagenesis kit with the following primer pairs: 5′-CCA CCC GCA CCT ACG AGC TGG GCA GCG CGC T-3′ and 5′-AGC GCG CTG CCC AGC TCG TAG GTG CGG GTG G-3′ to generate S38E mutation; 5′-CCA CCC GCA CCT ACG CCC TGG GCA GCG CGC-3′ and 5′-GCG CGC TGC CCA GGG CGT AGG TGC GGG TGG-3′ to generate S38A mutation; 5′-GGC TCC TGC AGG ACG AGG TGG ACT TCT CGC-3′ and 5′-GCG AGA AGT CCA CCT CGT CCT GCA GGA GCC-3′ to generate S83E mutation; 5′-GGC TCC TGC AGG ACG CGG TGG ACT TCT CGC-3′ and 5′-GCG AGA AGT CCA CCG CGT CCT GCA GGA GCC-3′ to generate S83A mutation.

2.2. Cell culture and transfection

All cells were cultured in Dulbecco's modified Eagle's medium (Gibco) supplemented with 10% fetal bovine serum (Gibco) at 37 °C with 5% CO_2. Huh7.5.1 cell line was a kind gift from Rongtuan Lin, McGill University (Canada). HEK293T (Cat# CRL-11268) cell line was purchased from ATCC. All knockout cell lines were generated by the CRISPR-Cas9 technology and cultured in DMEM with 10% FBS and 2 μg/mL puromycin

(Sangon Biotech). Plasmids were transfected into the cells by Lipofectamine 2000 (11668-019, Invitrogen) or Vigofect (T001, Vigorous), respectively, in accordance with the manufacturers' instructions.

2.3. Gene silencing

siRNAs were transfected into HEK293T and Huh7.5.1 cells using Lipofectamine™ RNAimax (13778-150, Invitrogen) with 50 pmol siRNA per well of 6-well plates. siRNAs were purchased from JSTBIO, non-targeted siRNA (siNT), target sequences 5′-UUC UCC GAA CGU GUC ACG UTT-3′ and 5′-ACG UGA CAC GUU CGG AGA ATT-3′; Vimentin-targeted siRNA (siVIM), target sequences 5′-UGA AGA AAC UCC ACG AAG ATT-3′ and 5′-UCU UCG UGG AGU UUC UUC ATT-3′; AKT-targeted siRNA (siAKT), target sequences 5′-GCA CCU UCA UUG GCU ACA ATT-3′ and 5′-UUG UAG CCA AUG AAG GUG CTT-3′.

2.4. HIV-1 and HCV infection

Vesicular stomatitis virus G protein (VSV-G)-pseudotyped HIV-1 NL4-3-Luc stocks were produced by transfecting HEK293T cells with pNL4-3-Luc-R-E- and pVSV-G at the ration of 2:1. Supernatants were harvested at 48 h post transfection, and cell debris was removed by low-speed centrifugation at 300×*g* (3-18K, Sigma, Osterode am Harz, Germany) for 5 min. HIV-1 p24 proteins were measured using an ELISA kit (Wantai BioPharm). VSVG-HIV-1 NL4-3-Luc containing 150 ng p24 was used to infect HEK293T cells. At 48 hpi, the cells were lysed for Western blotting (WB) analysis, detection of firefly luciferase activity using a Centro XS3 LB 960 Luminometer (Berthold), or integrated DNA measurement by RT-qPCR. Huh7.5.1 cells were seeded into 6-well plates, 4×10^5 per well, 24 h before transfection with plasmid expressing MXB or empty plasmid for 48 h. The cells were infected with JFH1 at an MOI of 0.5. Upon another 48 h, the cells were harvested and lysed for WB to measure the level of HCV core protein. Total RNA was extracted and applied for the subsequent intracellular HCV RNA analysis by RT-qPCR. 100 μL supernatants of cell culture-derived HCV (HCVcc)-infected cells were collected and incubated with 1×10^4/well naïve Huh7.5.1 cells seeded in a 96-well plate for another 48 h. Immunofluorescence analysis was used to stain HCV core protein in the cells and focus-forming units (PFU) were counted to measure extracellular HCV titer by IncuCyte S3 (Sartorius).

2.5. Co-immunoprecipitation (Co-IP)

For Co-IP analysis, virus-infected or plasmids-transfected cells were harvested for cell lysis by using the buffer [25 mmol/L Tris (pH = 7.4), 150 mmol/L NaCl, 1% NP-40, 1 mmol/L EDTA, and 5% glycerol (Pierce)] on ice. The lysates were centrifuged at 13,800×*g* (Pico 17, ThermoFisher, Osterode am Harz, Germany) for 10 min to remove cell debris. Then, 8% of the whole-cell lysates (8% WCL) examined by WB were used to measure protein expressions, and the other part of the lysates was incubated with specific antibodies and protein A+G agarose gel beads (P2012, Beyotime) overnight, under gentle agitation at 4 °C. After washing with the lysis buffer, the pull-down proteins were detected by WB. The proteins were then transferred onto 0.45 μm polyvinylidene difluoride membrane and incubated with primary antibodies. The antibodies used for WB included rabbit anti-VIM antibody (ab92547, Abcam), mouse anti-VIM antibody (ab8978, Abcam), rabbit anti-VIM S83 antibody (AP0799, ABclonal), rabbit anti-VIM S82 antibody (ab52943, Abcam), rabbit anti-VIM S72 antibody (ab52944, Abcam), rabbit anti-VIM S55 antibody (ab217673, Abcam), rabbit anti-VIM S38 antibody (ab52942, Abcam), rabbit anti-AKT antibody (ab8805, Abcam), rabbit anti-Flag antibody (D6W5B, CST), mouse anti-Flag antibody (9A3, CST), goat anti-Flag antibody (ab1257, Abcam), rabbit anti-HA antibody (C29F4, CST), rabbit anti-MXB antibody (A83265, NOVUS), mouse anti-actin antibody (AC004, ABclonal), mouse anti-PDI antibody (ab2792, Abcam), rabbit anti-p84 antibody (ab131268, Abcam), rabbit anti-CYPA antibody (ab41684, Abcam), mouse anti-HCV core antibody (ab2740, Abcam), and rabbit anti-HIV-1 p24 antibody (ab9071, Abcam). After probing with specific antibodies, the membrane was further incubated with secondary antibodies, including HRP-conjugated goat anti-mouse (ZB2305, ZSGB-Bio), goat anti-rabbit (ZB2301, ZSGB-Bio), or rabbit anti-goat (ZB2306, ZSGB-Bio). The protein signals were detected by the ChemiDoc MP imaging system (Bio-Rad). The relative protein band intensities were quantified using the ImageJ Gel Analyser.

2.6. RT-qPCR

HCV and HIV-1 RNA were extracted from infected cells using an RNA extraction kit (71202-50, Tiandz) and then examined using RT-qPCR analysis with a one-step RT-PCR kit (RR066A, Takara) following the manufacturer's specifications. The HCV primer pair: 5′-GCG TTA GTA TGA GTG TCG TG-3′ and 5′-TCG CAA GCA CCC TAT CAG-3′; the late HIV-1 DNA primer pair: 5′-TGT GTG CCC GTC TGT TGT G-3′ and 5′-GAG TCC TGC GTC GAG A-3′; the AKT primer pair: 5′-TTC TGC AGC TAT GCG CAA TGT G-3′ and 5′-TGG CCA GCA TAC CAT AGT GAG GTT-3′; the glyceraldehyde-3-phosphate dehydrogenase (GAPDH) primer pair: 5′-ATC ATC CCT GCC TCT ACT GG-3′ and 5′-GTC AGG TCC ACC ACT GAC AC-3′; the results of GAPDH served as an internal control to normalize the target RNA. The integrated DNA of HIV-1 was first amplified with the primer pair 5′-GCC TCC CAA AGT GCT GGG ATT ACA G-3′ and 5′-GTT CCT GCT ATG TCA C TT CC-3′, which targeted the domain of Alu and HIV-1 Gag DNA, followed by a secondary PCR with primers 5′-TTA AGC CTC AAT AAA GCT TGC C-3′ and 5′-GTT CGG GCG CCA CTG CTA GA-3′, which was probed with HIV-1 long terminal repeat (Alu-PCR).

2.7. Immunofluorescence staining

The transfected or infected cells were fixed with 4% paraformaldehyde for 20 min, permeabilized with 0.02% Triton X-100 (Thermo) for 8 min, and then blocked with 2% BSA (Sigma) for 1 h at room temperature, followed by incubating with primary antibodies for another 1 h with gentle shaking. After washing with PBS, secondary antibodies (Alexa Fluor 488−donkey anti-mouse, Alexa Fluor 555−donkey anti-rabbit, and Alexa Fluor 640−donkey anti-goat (Invitrogen)) were further applied for incubation. To stain the nuclei, 4′,6-diamidino-2-phenylindole (DAPI) (ZSGB-Bio) was used. Images were recorded with an Ultra View VoX confocal microscope (PerkinElmer) using a 100 × oil objective.

2.8. *In situ proximity ligation assay (PLA)*

PLA assay was performed using Duolink PLA starter kits (DUO92101, Sigma) according to the manufacturer's protocol. Briefly, Huh7.5.1 cells were transfected with plasmids expressing MXB-Flag or MXB-Flag (26−715) for 48 h and then fixed with 4% paraformaldehyde for 30 min and permeabilized with 0.02% Triton X-100. The cells were incubated with a blocking solution for 1 h. Primary antibodies were used to incubate the fixed cells for 1 h at 37 °C. The cells were further incubated with donkey anti-mouse and donkey anti-rabbit secondary antibodies conjugated with Duolink PLA minus and plus oligonucleotide probes for 1 h; next, the cells were incubated with a ligation solution for 30 min at 37 °C after washing with buffer A. The amplification solution was used to amplify the ligated PLA probes for 100 min, which was followed by washing with wash buffer B. Finally, the cells were mounted with Duolink PLA mounting medium containing DAPI. Fluorescence signals were using a PerkinElmer Ultra View VoX confocal microscope with a 100× oil objective.

2.9. *Liquid chromatography mass spectrometry (LC−MS)/MS-based label-free quantitative proteomics analysis*

2.9.1. *Proteins processing*

IFN-α2b-treated cells or cells with MXB overexpressing were suspended in the lysis buffer (8 mol/L urea, 1% protease inhibitor cocktail) and then sonicated three times on ice by a high-intensity ultrasonic processor (Scientz). The cell debris was removed by centrifugation at 12,000 × *g* (Pico 17, ThermoFisher, Osterode am Harz, Germany) for 10 min. The concentrations of proteins in supernatants were then determined with a BCA kit according to the manufacturer's instructions. Then the supernatants were treated with 5 mmol/L dithiothreitol for 30 min at 56 °C and alkylated with 11 mmol/L iodoacetamide for 15 min at room temperature in darkness. To down-regulate the urea concentration to less than 2 mol/L, the protein samples were diluted with 100 mmol/L TEAB. Trypsin was added to protein at the ratio of 1:50 for the primary digestion overnight; for a secondary digestion, the 1:100 trypsin-to-protein ratio was used. Finally, the peptides were desalted by C18 SPE column.

2.9.2. *LC−MS/MS analysis*

The tryptic peptides were dissolved in solvent A (0.1% formic acid, 2% acetonitrile/in water) and loaded onto a home-made reversed-phase analytical column (25 cm length, 75/100 μm i.d.). The peptides were separated with a gradient from 6% to 24% solvent B (0.1% formic acid in acetonitrile) over 70 min; 24%−35%, 14 min; and climbing to 80% in 3 min, then holding at 80% for the last 3 min, all at the constant flow rate of 450 nL/min on a nanoElute UHPLC system (Bruker Daltonics). The peptides were subjected to the capillary source, and then followed by the timsTOF Pro (Bruker Daltonics) mass spectrometry. Fragments were analyzed using a TOF detector under the scan range from *m/z* 100 to 1700. The electrospray voltage was 1.60 kV. Parallel accumulation serial fragmentation mode was used in the timsTOF Pro. Precursors with charge states 0 to 5 were selected for fragmentation, and 10 PASEF-MS/MS scans were acquired per cycle. The dynamic exclusion was set to 30 s.

2.9.3. *Database search*

The data were processed using the MaxQuant search engine (v.1.6.15.0). Tandem mass spectra were searched against the human SwissProt database (20395 entries). Trypsin/P was set as the cleavage enzyme. The length of peptides was set at over 7 amino acids. The maximum modifications of peptides were set as 5. The mass tolerance for precursor ions was set at 20 ppm in the first search and 20 ppm in the main search, and that of fragment ions was set at 20 ppm. Carbamidomethyl on cysteine was treated as fixed modification; in addition, oxidation on methionine and acetylation on protein N-terminus were selected as variable modifications. FDR was adjusted to <1%. The raw data were processed by the GO pathway enrichment. The identified proteins were annotated into the following three GO categories: biological processes, cellular components, and molecular function using eggnog-mapper software (v2.0) based on the EggNOG database. For each category, a two-tailed Fisher's exact test was run to test the enrichment of the differentially expressed protein against all identified proteins, where GO descriptions with a corrected *P*-value <0.05 were considered significant.

2.10. *Statistical analyses*

All data are presented as means ± Standard Error of the Mean (SEM). Statistical analyses were performed with two-tailed, unpaired Student's *t* test and multiple *t* tests available in GraphPad Prism software. Significant differences were marked as $^{*}P < 0.05$; $^{**}P < 0.01$; $^{***}P < 0.001$; n.s., not significant.

3. Results

3.1. *IFN-mediated change in host protein subcellular distribution is partially corrected with MXB depletion*

We first examined the effect of IFN treatment on the subcellular distribution of host proteins using the proteomics approach. Briefly, subcellular fractions of HEK293T cells with or without IFN treatment were prepared, which was followed by a LC−MS/MS-based label-free quantitative proteomics analysis. A total of 8001 proteins were detected (the list of identified proteins is available upon request). Among these proteins, the abundance of 806 and 543 proteins in the nuclear and cytoplasmic membrane fractions, respectively, changed by more than 2-fold ($P < 0.05$) upon IFN treatment (Supporting Information Fig. S1). The results of the GO pathway enrichment analysis revealed that most of the altered genes were enriched in the pathways of nucleoside phosphate metabolism, carboxylic acid metabolism, ribose phosphate metabolism, DNA metabolism, and negative regulation of cell cycle (Fig. 1A and C). After comparing the total protein levels in the whole cell lysates with and without IFN treatment, we found that the treatment did not change the expression levels of about 97% of proteins that varied in nuclear and cytoplasmic membrane fractions. This finding suggests that the changed subcellular abundance is not a result of altered expression of the proteins upon IFN stimulation. Instead, these data highlight a global effect of IFN treatment on the subcellular distribution of host proteins.

We next investigated protein subcellular distribution in MXB-knockdown cells in response to IFN treatment using the same LC−MS approach, to investigate the potential role of MXB in IFN altering protein subcellular distribution. As shown in Fig. S1, in response to IFN treatment, knocking down MXB abolished the changes in the abundance of 349 and 163 proteins in the nuclear and membrane fractions. The results of the GO pathway

enrichment analysis showed that these MXB-dependent genes were enriched in pathways of regulation of lipid metabolism, oxidative phosphorylation, vesicle organization, and negative regulation of cell cycle (Fig. 1B and D). Collectively, these data suggest that IFN may modulate protein subcellular distribution as a result of altering intracellular protein transportation and trafficking, and that this function of IFN, to a significant extent, depends on MXB.

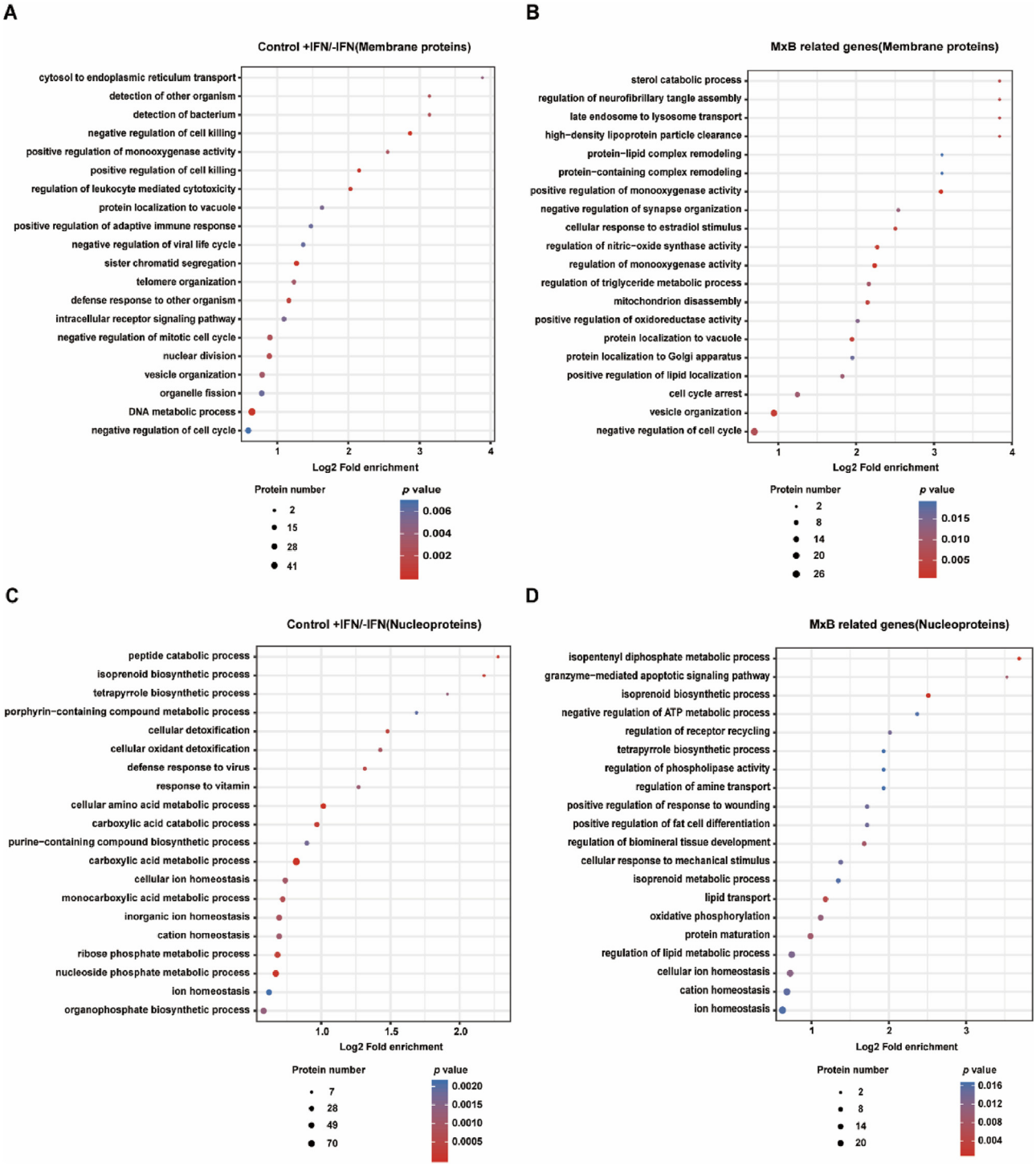

Figure 1 MXB participates in IFN-mediated regulation of protein subcellular distribution. Prior to fractionation with the subcellular protein fractionation kit (Pierce), HEK293T and HEK293T $MXB^{-/-}$ cells were treated with IFN-α2b (500 IU/mL). Two cellular fractions (cytoplasmic membrane fraction and nuclear fraction) were respectively isolated; the former included plasma, mitochondria, and ER/Golgi membranes, while the latter corresponded to soluble nuclear contents. Proteins in the subcellular fractions were determined by LC−MS. The raw data were processed by GO pathway enrichment, $n = 3$. (A) GO pathway enrichment of total cytoplasmic membrane fractions. (B) GO pathway enrichment of MXB-related proteins in cytoplasmic membrane fractions. (C) GO pathway enrichment of nuclear fractions. (D) GO pathway enrichment of MXB-related proteins in nuclear fractions.

3.2. *MXB interacts with intermediate filament VIM*

In order to understand how MXB regulates intracellular protein transportation and trafficking in response to IFN, we first performed *Escherichia coli* biotin ligase (BirA)-mediated proximity-dependent biotin identification (BioID), coupled with the MS approach to identify cellular proteins that associated with MXB. In brief, the BirA sequence was attached to the C-terminus of the wild-type MXB or the N-terminal truncated MXB (92−715). HEK293T cells that expressed MXB-BirA or MXB (92−715)-BirA were exposed to biotin to label proteins that were in close contact with MXB-BirA or MXB (92−715)-BirA; the biotin-labeled proteins were isolated with streptavidin beads and determined by mass spectrometry. Since early studies reported that the N-terminus of MXB is indispensable for its biological functions such as the antiviral activity[36], the truncated form of MXB (92−715) was used as a control. The results revealed that 196 MXB-associated proteins were absent or had a significantly low level in the control samples (Supporting Information Table S1).

Notably, the intermediate filament protein VIM was the top candidate interacting with MXB, but not with MXB (92−715) (Fig. 2A). In previous research, intermediate filament was found to regulate intracellular protein trafficking and may assist the virus to transport to its replication site within cells[48,49]. Accordingly, we performed experiments to verify and further characterize the interaction of VIM with MXB. The results of two-way Co-IP confirmed that the ectopically expressed MXB, not its MXB (26−715) mutant, interacted with endogenous VIM (Fig. 2B). This observation was supported by the data of PLA where protein interactions were detected as individual fluorescent dots and revealed interactions between MXB and VIM both in the cytoplasm and around the nucleus (Fig. 2C). Next, we used IFN to treat cells and evaluated the interaction of IFN-induced endogenous MXB with VIM. Again, the endogenous MXB was found to

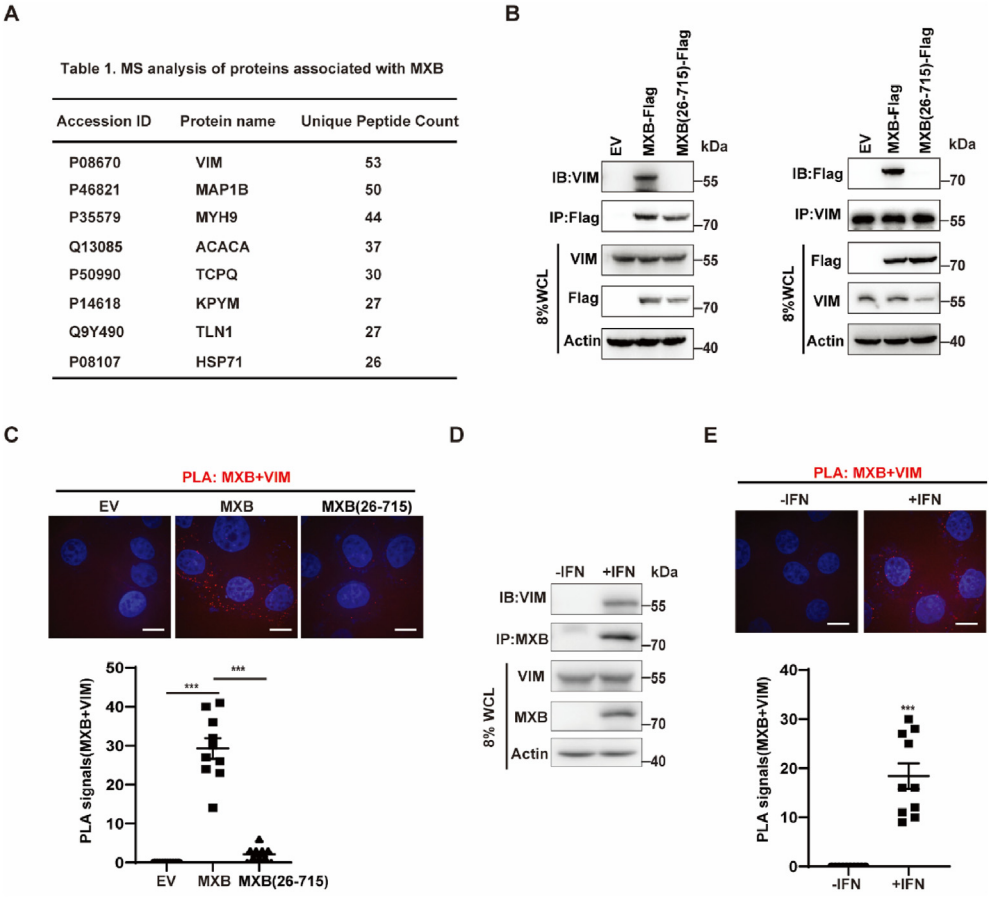

Figure 2 MXB interacts with VIM. (A) Table 1 lists the top candidates associated with MXB as identified by BioID and MS analysis, $n = 3$. (B) HEK293T cells were transfected with MXB-Flag or MXB (26−715)-Flag plasmid, and empty vector (EV) was used as a negative control. Then the cell lysates were subject to immunoprecipitation (IP) with anti-Flag or anti-VIM antibody. Immunoblot (IB) was probed with anti-VIM or anti-Flag antibody. Next, 8% WCL were immunoblotted to show the expression of MXB-Flag, MXB (26−715)-Flag, and VIM. Three independent experiments were performed. (C) Huh7.5.1 cells were transfected plasmids expressing MXB-Flag or MXB (26−715)-Flag. Association of MXB with VIM was examined with in situ PLA and detected as red puncta within the cells. The red puncta were scored in randomly selected cells ($n = 10$) using the Image-Pro Plus 7.0C software; the data were plotted as a grouped column scatter diagram. Representative images are shown. Bars, 10 μm. (D) HEK293T cells were treated with IFN-α2b (500 IU/mL) for 48 h, and the cell lysates were subject to IP with anti-MXB antibody. The presence of VIM was detected in IB, $n = 3$. (E) Huh7.5.1 cells were treated with IFN-α2b (500 IU/mL) for 48 h. The association of MXB with VIM was examined with PLA. Randomly selected cells ($n = 10$) were examined to score the red puncta. Bars, 10 μm. The significance of difference is indicated as $^{***}P < 0.001$.

associate with VIM in the Co-IP experiment (Fig. 2D) and in the PLA study (Fig. 2E). Together, these results demonstrate that MXB interacts with VIM.

3.3. *Depleting VIM abrogates MXB inhibition of HIV-1 and HCV*

To examine the potential role of VIM in the antiviral activity of MXB, we knocked down VIM with siRNA in HEK293T cells that were transfected to express MXB-Flag protein, followed by infection with VSV-pseudotyped HIV-1 NL4-3-Luc that expressed luciferase upon a successful infection. Consistently with previous reports, MXB inhibited HIV-1 replication by approximately 50%[50]. Of note, as compared with 80%−90% inhibition on wild type HIV-1 or pseudotyped HIV-1 by MXB in T lymphocytes, much less potency of MXB in VSV-pseudotyped HIV-1 infected non-lymphocytes was generally observed, which could have been due to the fact that non-lymphocytes tend to be more sensitive to these pseudotyped viron[51]. In addition, we found that knockdown of VIM abolished MXB-mediated inhibition of HIV-1 infection (Fig. 3A). This observation was verified by the data produced with the cells with VIM knocked out using CRISPR-Cas9 (Fig. 3B). We further measured MXB inhibition of HCV infection with knockdown or knockout of VIM and observed the loss of HCV

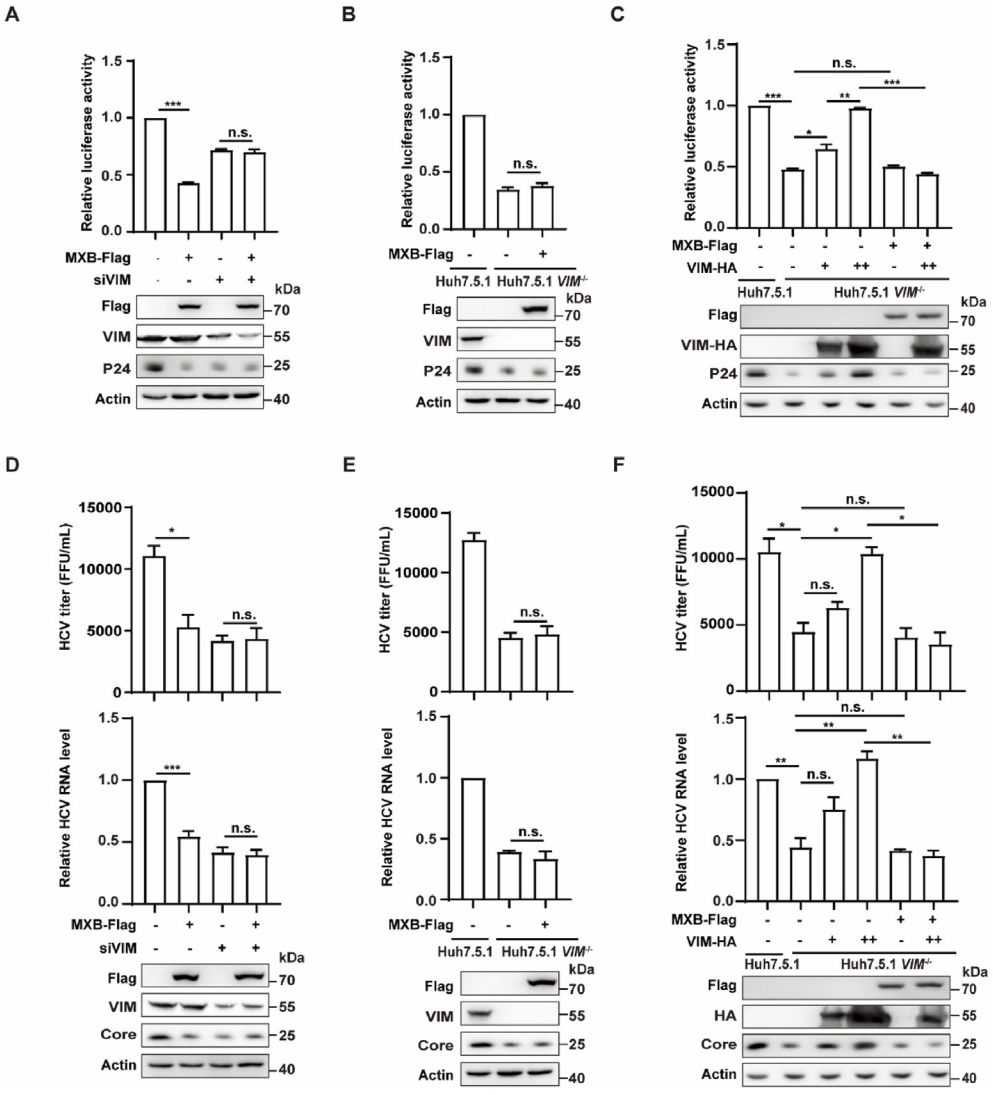

Figure 3 MXB inhibition of HIV-1 and HCV depends on VIM. (A, D) Huh7.5.1 cells were cotransfected with either siVIM or siNT and MXB-Flag plasmid DNA, followed by the infection with VSV-pseudotyped HIV-1 NL4-3-Luc (A) or JFH1 HCVcc (D). Expression of MXB and VIM was determined by WB. HIV-1 infection was evaluated by measuring firefly luciferase activity and expression of HIV-1 p24. HCV infection was measured by detecting extracellular HCV titer, intracellular viral RNA, and HCV core protein. The data shown here represent at least three independent experiments. The values are expressed as means ± SEM. (B, E) Huh7.5.1 $VIM^{-/-}$ cells were transfected with MXB-Flag plasmid DNA and infected with VSV-pseudotyped HIV-1 NL4-3-Luc (B) or JFH1 HCVcc (E). HIV-1 and HCV infection were determined using the same methods as (A) and (D); the data are presented as means ± SEM, $n = 3$. (C, F) Huh7.5.1 $VIM^{-/-}$ cells were transfected or co-transfected with plasmid expressing VIM-HA and MXB-Flag, then infected with VSV-pseudotyped HIV-1 NL4-3-Luc (C) or JFH1 HCVcc (F). HIV-1 and HCV infection were evaluated, respectively. The data represent at least three independent experiments. The values are expressed as means ± SEM. For all panels, the data were normalized to the control group, with the control value arbitrarily set to 1. The significance of difference is indicated as $*P < 0.05$, $**P < 0.01$, $***P < 0.001$; n.s., not significant.

inhibition by MXB (Fig. 3D and E). The overexpression of VIM significantly rescued the infection of HIV-1 and HCV and restored the antiviral activity of MXB in VIM-KO cells (Fig. 3C and F). We also noted that reducing VIM expression alone decreased the infection of HIV-1 and HCV by about 50%; MXB did not further reduce viral infection, suggesting that, rather than assisting MXB to inhibit HIV-1 and HCV, VIM serves as a cofactor of HIV-1 and HCV infection and is likely targeted and negated by MXB.

3.4. *VIM assists HIV-1 and HCV infection*

Considering that MXB impairs nuclear import of HIV-1 DNA and the localization of HCV NS5A to ER[10,43], we speculated that VIM may play a role in these transport events of viral molecules. Indeed, depletion of VIM resulted in a significant reduction in the integrated HIV-1 DNA, but not in the viral cDNA synthesis that occurs within the cytoplasm, as shown by the results of RT-qPCR in Fig. 4A and B. These findings support a positive role of VIM in the translocation of HIV-1 DNA from the cytoplasm into the nucleus, although the possibility that VIM may participate in HIV-1 DNA integration can not be ruled out. Furthermore, VIM knockdown significantly reduced the colocalization of NS5A with ER marker protein disulfide isomerase (PDI) (Fig. 4C), further supporting the role of VIM in the intracellular transport of viral molecules and complexes.

Several previous studies reported MXB-resistant HIV-1 capsid (such P90A) and HCV NS5A (D316E and Y317N(DEYN)) mutants[52,53]. In our results, in contrast to the wild type viruses, viral DNA integration of the P90A HIV-1 mutant and ER localization of HCV NS5A DEYN mutant were not affected by VIM depletion (Fig. 4D and E). The correlation between viral sensitivity to MXB and the viral dependence on VIM suggests that MXB may inhibit viruses by impairing the function of VIM in mediating intracellular transport of key viral molecules and complexes. In support of this hypothesis, we found that the P90A HIV-1 capsid mutant lost association with VIM, as shown by the PLA data in Fig. 4F. Similarly, HCV NS5A DEYN mutant no longer formed a complex with VIM (Fig. 4G).

We and others reported that MXB inhibition of HIV-1 and HCV depends on CYPA[10,44]. To test possibility that CYPA may participate in VIM-mediated intracellular transport of viral molecules, we examined the association of HIV-1 capsid and HCV NS5A with VIM in CYPA-KO cells by performing PLA and observed substantial loss of VIM association with these viral proteins as compared to that in control cells (Fig. 4F and G). This loss of association was further supported by the results of Co-IP experiment on the interaction between NS5A and VIM in the presence or absence of CYPA (Fig. 4H). Taken together, these data demonstrate that VIM supports the intracellular transport of HIV-1 capsid and HCV NS5A in a CYPA-dependent manner.

3.5. *MXB causes a rearrangement of VIM network as a result of VIM phosphorylation at amino acid S38*

To test the hypothesis that MXB inhibits HIV-1 and HCV by abrogating VIM-mediated intracellular transport of key viral molecules, we first examined the effect of MXB on the subcellular distribution of VIM. The results of immunofluorescence assays revealed that, as opposed to the diffuse distribution of VIM in control cells, MXB expression caused a greater aggregation of VIM (Fig. 5A). Similarly, IFN-α2b treatment caused VIM aggregation, which was not observed in MXB-KO cells with IFN-α2b treatment (Fig. 5B). These data suggest that MXB modulates the organization of VIM network. Of note, only partial VIM was found colocalization with MXB (Fig. 5A), while VIM-associated viral replication was completely blocked by over-expressed MXB (Fig. 3). These observations raise the possibilities that either MXB−VIM interaction is dynamic and reversible, or MXB may target only the group of VIMs participating in intracellular transport of viral proteins; these possibilities warrant further investigation.

VIM network organization is affected by various post-translational modifications, including phosphorylation at amino acid positions S38, S55, S71, S82, and S83[54,55]. We thus investigated whether MXB affects VIM phosphorylation at the above amino acid positions by performing WB using antibodies specific for different phosphorylation sites of VIM. The results revealed that MXB increased phosphorylation of VIM specifically at S38, but not at any of the other sites (Fig. 5C). In support of this observation, IFN treatment also increased the phosphorylation of S38 in VIM, and this increased S38 phosphorylation of VIM was not observed in MXB-KO cells with IFN treatment (Fig. 5D). Therefore, it can be concluded that MXB expression leads to phosphorylation of VIM at amino acid S38.

To further examine the role of S38 phosphorylation in VIM network organization, we generated the phospho-mimetic mutation S38E and the non-phosphorylation mutation S38A. The S38E VIM mutant exhibited the aggregation distribution in VIM-KO cells as opposed to the non-phosphorylation mutant S38A that exhibited the diffuse distribution and, importantly, did not aggregate with MXB expression (Fig. 5E). Used as a control, the S83A VIM mutant transformed from diffuse distribution to aggregation by MXB. Together, these results demonstrate that MXB causes VIM phosphorylation specifically at S38, which leads to a VIM network reorganization.

3.6. *MXB-induced phosphorylation of VIM at S38 impairs viral replication*

To investigate the effect of MXB-induced S38 phosphorylation of VIM on viral infection, we used HIV-1 and HCV to infect *VIM*$^{-/-}$ cells supplemented with HA-tagged VIM or its mutants; next, HIV-1 DNA integration and HCV NS5A ER-localization were measured. The results revealed that, similarly to the wild type VIM, non-phosphorylation mutants S38A and S83A were all able to increase HIV-1 DNA integration and ER localization of HCV NS5A, as opposed to the phospho-mimetic S38E that did not exert any enhancing effect (Fig. 6A and B, and Supporting Information Fig. S2A). These data indicate that VIM with phosphorylated S38 cannot support viral replication. Finally, we investigated the role of S38 phosphorylation of VIM in the antiviral activity of MXB, and observed that in *VIM*$^{-/-}$ cells, the S38A mutant, but not S83A, rendered HIV-1 refractory to MXB inhibition (Fig. 6C). In addition, overexpression of VIM mutant S38A strongly resisted the MXB disruption of NS5A localization to ER (Fig. 6D and Fig. S2B). Together, we conclude that MXB inhibits HIV-1 and HCV infection by causing phosphorylation of VIM at S38.

3.7. *Cellular kinase AKT is responsible for MXB-induced phosphorylation of VIM at S38*

To determine which cellular kinases are recruited by MXB to phosphorylate VIM at S38, we tested inhibitors targeting ERK1/2, PAK, PKA, ROCK, or AKT that were previously

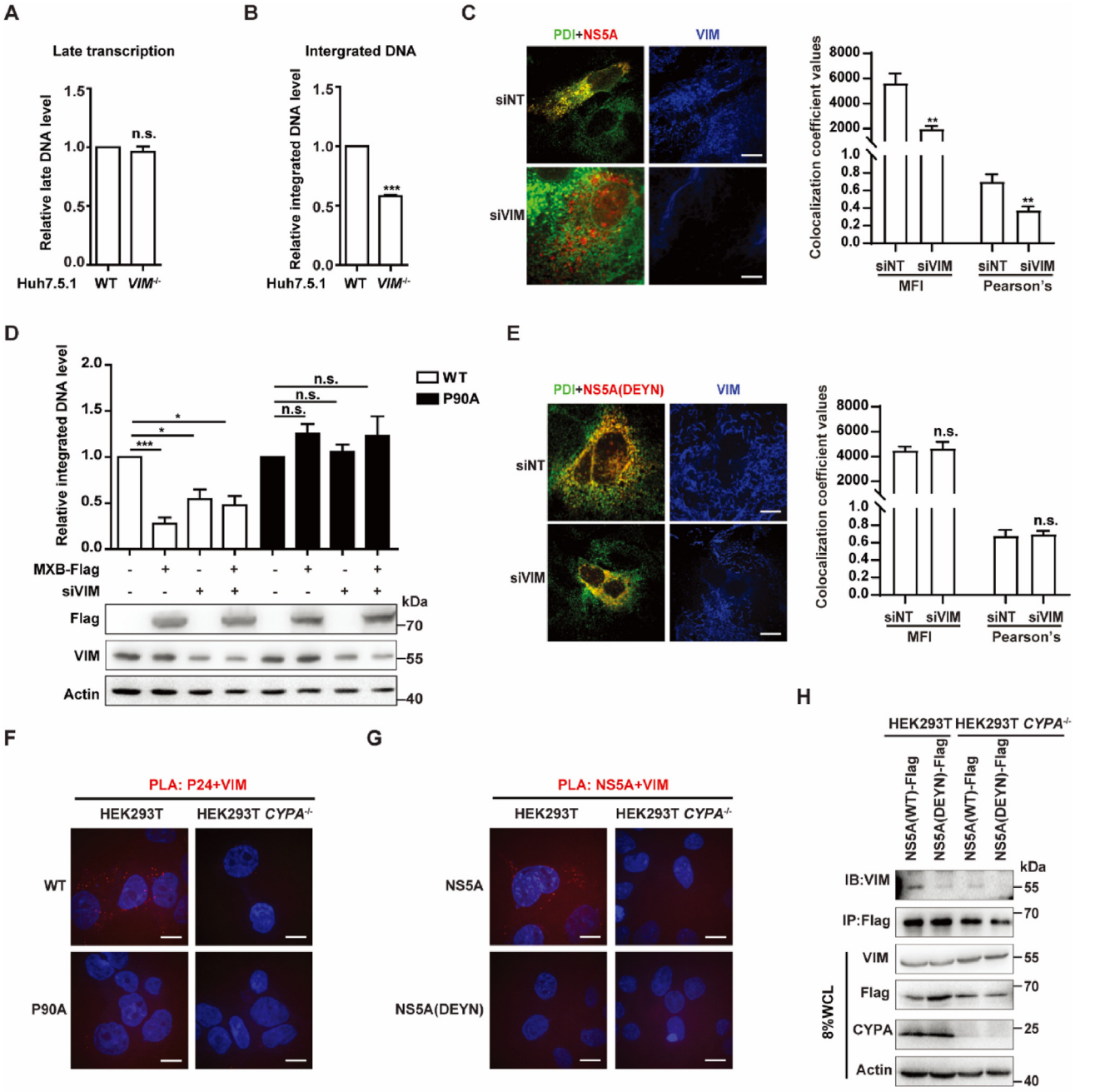

Figure 4 The role of VIM in HIV-1 and HCV infection. (A, B) Effects of VIM knockout on HIV-1 reverse transcription and integration. VSV-pseudotyped HIV-1 NL4-3-Luc was used to infect Huh7.5.1 or Huh7.5.1 *VIM*$^{-/-}$ cells. The amounts of late reverse transcription DNA products were determined by RT-qPCR (A). Levels of integrated HIV-1 DNA were measured by Alu-PCR (B). Data are presented as means ± SEM, $n = 3$. (C, E) Colocalization of PDI (ER marker) with HCV NS5A. Huh7.5.1 cells were transfected with siVIM and plasmid DNA expressing HCV NS5A (C) or HCV NS5A (DEYN) mutant (E). The cells were fixed and stained for PDI (green), NS5A (red) and VIM (blue). Representative images are shown, $n = 3$. Bars, 5 μm. The colocalization coefficient values (mean fluorescence intensity (MFI) and Pearson's values) were detected by using the Image-Pro Plus 7.0C software. Five images were randomly selected for colocalization analysis. (D) Effects of MXB overexpression and VIM knockout on the integration of HIV-1 and P90A mutant virus. HEK293T cells were cotransfected with either siVIM or siNT and plasmid expressing MXB-Flag, followed by the infection of VSV-pseudotyped HIV-1 NL4-3-Luc or mutant virus. HIV-1 DNA was extracted and the levels of integrated viral DNA were measured by Alu-PCR. The results in the figure show the average of three independent infection experiments. The data are presented as means ± SEM. (F) Wild type HEK293T cells and *CYPA*$^{-/-}$ cells were infected with VSV-pseudotyped HIV-1 NL4-3-Luc or the P90A mutant. The association of HIV-1 capsid with VIM was examined by PLA and detected as red puncta within cells. Bars, 10 μm. This experiment was performed in triplicate; the representative images are shown. (G) Wild HEK293T cells and HEK293T *CYPA*$^{-/-}$ cells were transfected with either NS5A or NS5A(DEYN) plasmid DNA. The association of HCV NS5A with VIM was examined by PLA and detected as red puncta within cells. Bars, 10 μm. This experiment was performed in triplicate; the representative images are shown. (H) Total lysates from wild HEK293T cells and HEK293T *CYPA*$^{-/-}$ cells were subject to immunoprecipitation with anti-Flag antibody. Immunoprecipitated complexes were examined using WB with anti-VIM antibody. Next, 8% WCL was immunoblotted to verify the expression of NS5A-Flag, VIM and CYPA ($n = 3$). The significance of difference is indicated as $^{*}P < 0.05$, $^{**}P < 0.01$, $^{***}P < 0.001$; n.s., not significant.

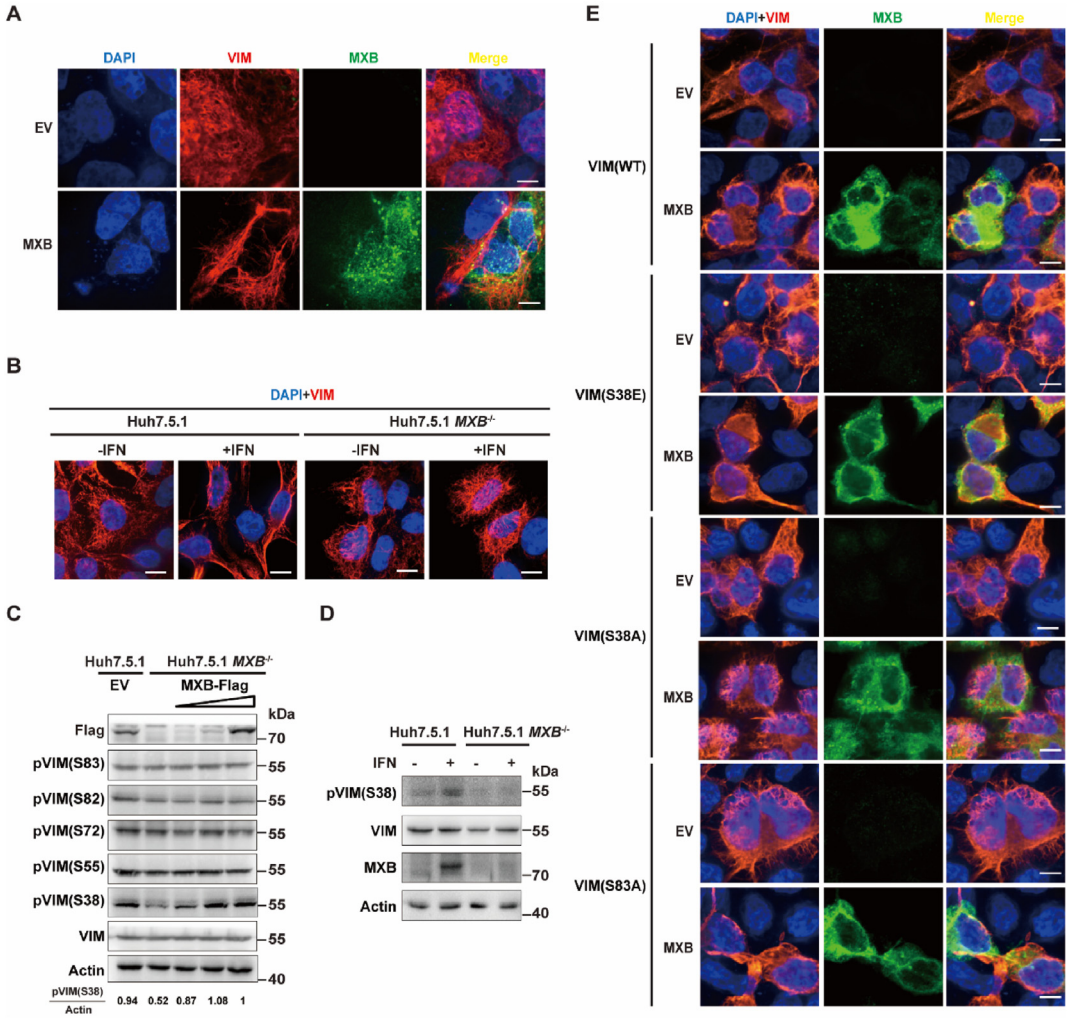

Figure 5 MXB regulates the VIM network by promoting phosphorylation at serine 38. (A) Huh7.5.1 cells were transfected with MXB-Flag plasmid or EV. MXB-Flag protein (green) and VIM (red) were visualized by immunostaining. The nuclei were stained by DAPI (blue). Representative images based on at least three independent experiments are shown. Bars, 5 μm. (B) Huh7.5.1 and Huh7.5.1 *MXB*$^{-/-}$ cells were treated with IFN-α2b (500 IU/mL) for 48 h. VIM (red) was immunostained, and the nuclei were stained by DAPI (blue) staining ($n = 3$). Bars, 5 μm. (C) Huh7.5.1 *MXB*$^{-/-}$ cells were transfected with EV or MXB-Flag plasmid DNA (0.5, 1, 2 μg), respectively. Wild type Huh7.5.1 cells transfected with EV were set as control. Expression Levels of endogenous MXB and phosphorylated VIM S38, S55, S72, S82, and S83 (pVIM(S38), pVIM(S55), pVIM(S72), pVIM(S82), pVIM(S83)) were determined by WB. The integrated density of pVIM(S38) and actin bands were measured by ImageJ and the ratio of pVIM(S38)/actin was calculated ($n = 3$). (D) Huh7.5.1 and Huh7.5.1 *MXB*$^{-/-}$ cells were treated with IFN-α2b (500 IU/mL) for 48 h. The level of pVIM(S38) was determined by WB ($n = 3$). (E) Huh7.5.1 *VIM*$^{-/-}$ cells were cotransfected with MXB-Flag and VIM-HA plasmid DNA or its mutants (S38E, S38A, and S83A). The cells transfected with EV and set as the control group. MXB protein (green) and HA tagged proteins (red) were visualized using immunostaining. Nuclei were stained with DAPI (blue). Representative images are shown ($n = 3$). Bars, 5 μm.

reported to be able to catalyze the phosphorylation of VIM at S38[56–58]. These inhibitors include ravoxertinib, IPA-3, H89·2HCl, Y-27632·2HCl, and MK-2206·2HCl targeting ERK1/2, PAK, PKA, ROCK and AKT, respectively. We first measured the effect of these inhibitors on the anti-HIV and HCV activity of MXB. The results showed that AKT, PKA, and ROCK inhibitors alone did not affect HIV-1 and HCV infection (Supporting Information Fig. S3), and restored the infection of HIV-1 and HCV in the presence of MXB to the levels in control cells (Fig. 7A and B), suggesting that inactivating AKT, PKA, or ROCK counteracts the antiviral effect of MXB. Among these three classes of inhibitors, only the AKT inhibitor MK-2206·2HCl inhibited the VIM S38 phosphorylation in MXB-overexpressing cells (Fig. 7C), suggesting that PKA and ROCK inhibitors antagonize MXB restriction by separate mechanisms (Supporting Information Fig. S4); importantly, these results also support the involvement of AKT in the MXB-induced VIM S38 phosphorylation. This possibility was further supported by the loss of S38 phosphorylation in VIM with MXB expression when AKT was knocked down (Fig. 7D). Moreover, either the AKT inhibitor treatment (Fig. 7E) or reducing AKT expression by siRNA (Fig. 7F) markedly restored the level of integrated HIV-1 DNA in MXB-expressing cells, whereas no significant effect on HIV-1 DNA integration in the cells without MXB was observed. In addition to the effect on HIV-1, the PLA data showed that AKT inhibitor dramatically restored the NS5A

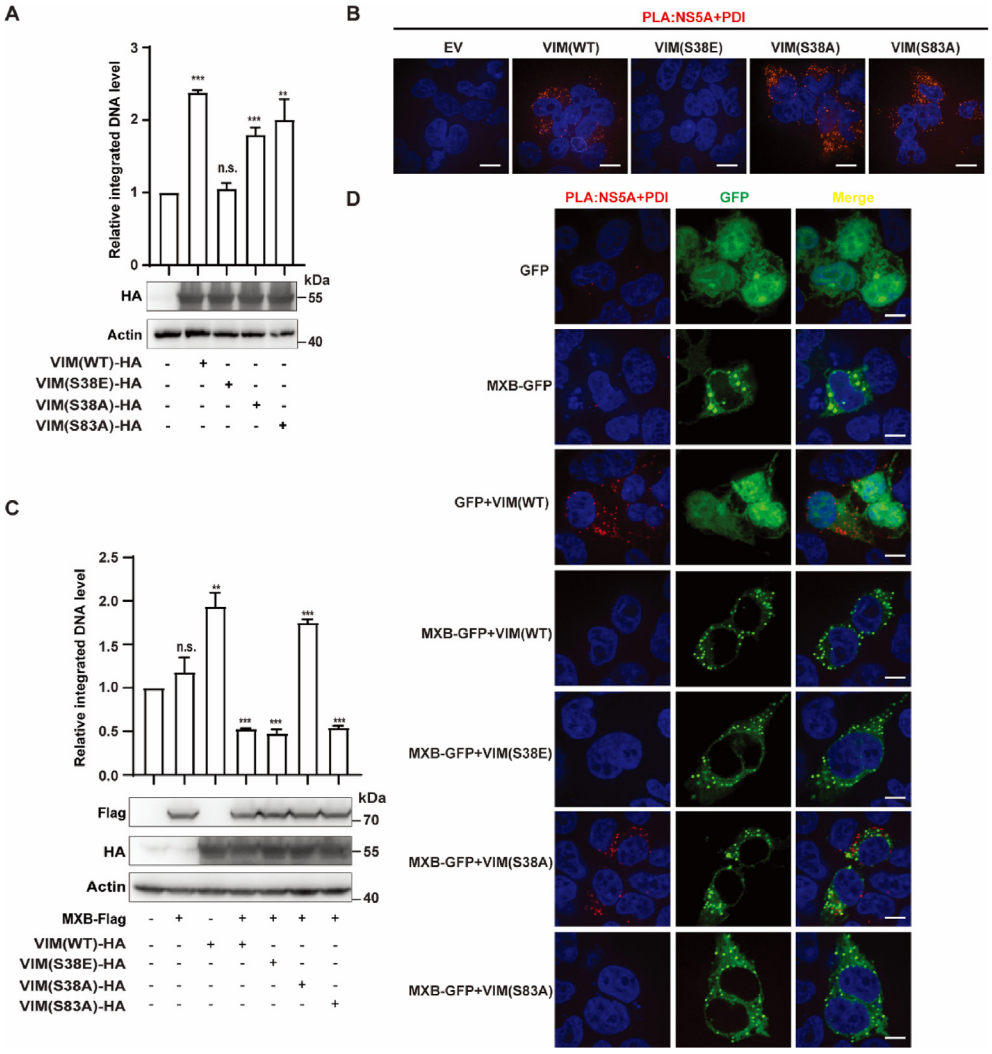

Figure 6 MXB-induced phosphorylation of VIM at S38 impairs viral replication. (A) Huh7.5.1 $VIM^{-/-}$ cells were transfected with plasmid DNA expressing either VIM-HA or its mutants (S38A, S38E and S83A), followed by the infection of VSVG-HIV-1 NL4-3. Levels of integrated viral DNA were measured by Alu-PCR. The results are presented in the bar graph; the data are presented as means ± SEM, $n = 3$. (B) Huh7.5.1 $VIM^{-/-}$ cells were cotransfected with plasmids expressing HCV NS5A-Flag and either VIM-HA or its mutant. The association of HCV NS5A with PDI was examined with PLA and detected as red puncta within cells. Bars, 10 μm. Three independent experiments were performed. (C) Huh7.5.1 $VIM^{-/-}$ cells were cotransfected with plasmid DNA expressing MXB-Flag and either VIM-HA or its mutants, followed by the infection of VSVG-HIV-1 NL4-3. The levels of integrated viral DNA were measured using Alu-PCR. The results are presented in the bar graph. The data are shown as means ± SEM, $n = 3$. (D) Huh7.5.1 $VIM^{-/-}$ cells were cotransfected with plasmid DNA expressing HCV NS5A-Flag, MXB-GFP, and either VIM-HA or its mutant. GFP plasmid was used as the control. The association of HCV NS5A with PDI was visualized as red puncta, and MXB was pseudocolored as green ($n = 3$). Bars, 5 μm. The significance of difference is indicated as $^{**}P < 0.01$, $^{***}P < 0.001$; n.s., not significant.

and PDI interaction in the presence of MXB, as compared with that in the cells without the treatment (Fig. 7G). Collectively, these findings suggest that AKT is required for MXB-induced phosphorylation of VIM at S38 and for MXB antiviral activity.

3.8. *MXB mediates the interaction between AKT and VIM*

To understand how MXB enables VIM phosphorylation by AKT, we first measured the levels of AKT protein and its mRNA, and did not observe significant change in the presence of MXB overexpression (Supporting Information Fig. S5). Instead, much higher amounts of AKT were co-immunoprecipitated with VIM in either the control or MXB-KO Huh7.5.1 cells with overexpressed MXB (Fig. 8A), suggesting that MXB promotes AKT association with its substrate VIM. In further support of this observation, the IFN treatment markedly increased AKT association with VIM, and this association was virtually lost in MXB-KO cells, as shown by the results of Co-IP (Fig. 8B) and PLA experiments (Fig. 8C). This lost AKT and VIM association in MXB-KO cells was restored with ectopic expression of MXB (Fig. 8A). Together, these results demonstrate a key role of MXB in AKT interaction with VIM. We also tested the MXB (26−715) mutant that lost the ability of binding to VIM (Fig. 2B), to find that this mutant was unable to promote AKT association with VIM nor restore the association of AKT with VIM in either the control or the MXB-KO cells (Fig. 8A). These results suggest that binding to VIM is

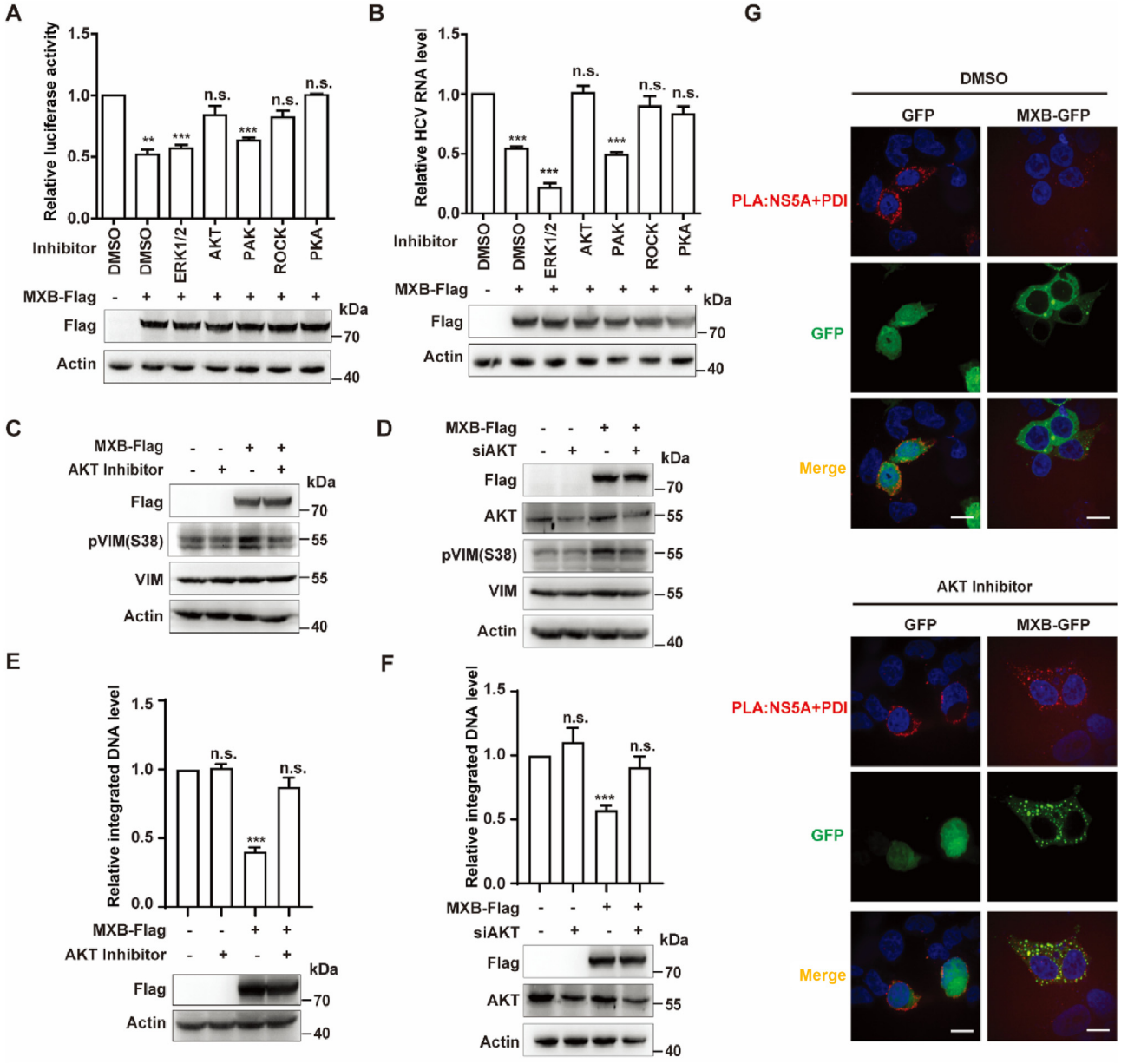

Figure 7 AKT participates in MXB-induced phosphorylation of VIM at S38. (A, B) HEK293T and Huh7.5.1 cells were transfected with MXB-Flag plasmid DNA and then treated with cellular kinase inhibitors. At 24 h after treatment, the cells were infected with VSVG-HIV-1NL4-3 (A) or JFH1 HCVcc (B). The infectivity of HIV-1 and HCV were evaluated by measuring firefly luciferase activity and viral RNA level, respectively. The data represent at least three independent experiments, and the values are expressed as means ± SEM. For all panels, data were normalized to the control group, with the control value set to 1. (C, D) HEK293T cells were transfected with MXB-Flag plasmid DNA and treated with either MK-2206 2HCl (C) or siRNA targeting AKT (D). The level of VIM phosphorylation at S38 was determined by WB ($n = 3$). (E, F) HEK293T and Huh7.5.1 cells were transfected with MXB-Flag plasmid DNA and treated with MK-2206 2HCl (E) or siRNA targeting AKT (F). At 24 h after treatment, the cells were infected with VSVG-HIV-1 NL4-3. The data represent at least three independent experiments, and the values are expressed as mean ± SEM. (G) Huh7.5.1 cells were cotransfected with NS5A-Flag and MXB-GFP plasmid DNA in the presence of MK-2206·2HCl. The association of HCV NS5A-Flag with PDI was examined using PLA and detected as red puncta; MXB was pseudocolored as green. Representative images are shown. Bars, 10 μm. This experiment was repeated in triplicate; the representative images are shown. The significance of difference is indicated as $^{**}P < 0.01$, $^{***}P < 0.001$; n.s., not significant.

required for MXB to enable AKT and VIM interaction. Therefore, we asked whether MXB is also capable of interacting with AKT and serves as a bridge to form the AKT−MXB−VIM complex. Indeed, the results of both of Co-IP and PLA experiments showed binding of MXB to of AKT. Importantly, VIM knockout did not affect the AKT−MXB interaction (Fig. 8D and E and Supporting Information Fig. S6). Along with the first 25 amino acids of MXB, other N-terminal consisting of GTPase domain and proline rich domain (MXB (26−334)), but not C-terminal (MXB (335−715)), also helped this interaction (Fig. 8D and E, and Supporting Information Fig. S7A). AlphaFold-Multimer v3 prediction suggested that MXB (1−25) (visually distinguished in blue) interjects

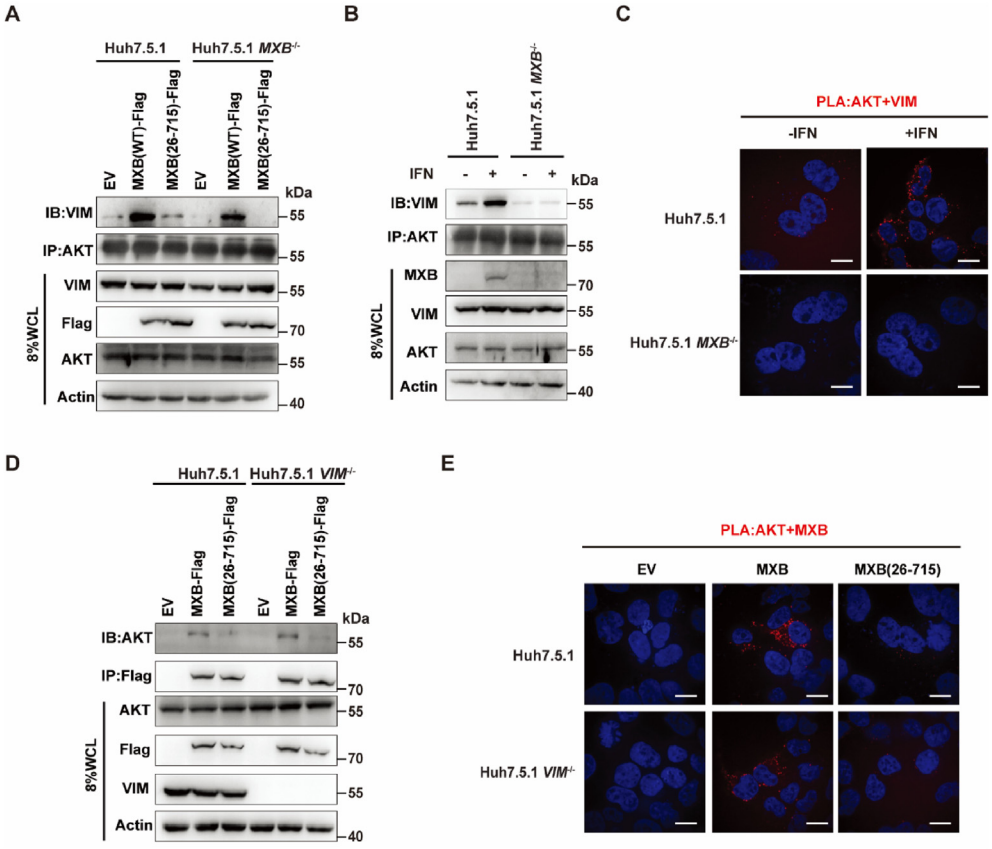

Figure 8 MXB mediates the interaction between AKT and VIM. (A) Huh7.5.1 cells or Huh7.5.1 *MXB*$^{-/-}$ cells were transfected with MXB-Flag or MXB (26−715)-Flag plasmid DNA. Total cell lysates were immunoprecipitated with anti-AKT antibody. Immunoprecipitated complexes were probed in IB with anti-VIM antibody. The data are representative of three independent experiments. (B) Total lysates of the control Huh7.5.1 or Huh7.5.1 *MXB*$^{-/-}$ cells, treated with IFN-α2b (500 IU/mL), were immunoprecipitated with anti-AKT antibody. The presence of VIM in the immunoprecipitated complexes was detected in IB with anti-VIM antibody ($n = 3$). (C) The association of VIM with AKT in Huh7.5.1 and Huh7.5.1 *MXB*$^{-/-}$ cells was examined with PLA. This experiment was repeated in triplicate. The interaction between VIM and AKT was detected as red puncta. Bars, 10 μm. The representative images are shown. (D) Total lysates from Huh7.5.1 or Huh7.5.1 *VIM*$^{-/-}$ cells, transfected with either MXB-Flag or MXB (26−715)-Flag plasmid DNA, were immunoprecipitated with anti-Flag antibody. Immunoprecipitated complexes were examined in IB with the anti-AKT antibody. Total expression of MXB-Flag, MXB (26−715)-Flag, VIM, and AKT were examined in 8% WCL. The data are representative of three independent experiments. (E) Interaction between MXB (or MXB (26−715)) and AKT was measured using PLA in Huh7.5.1 and Huh7.5.1 *VIM*$^{-/-}$ cells. Three independent experiments were performed, and representative images are shown. Bars, 10 μm.

itself between AKT and VIM. This specific arrangement serves as an anchor, facilitating a stable structural association of these two proteins within the complex and suggesting that N-terminal of MXB plays an important role in connecting AKT and VIM (Fig. S7B). Together, we conclude that MXB acts as a bridge to mediate the interaction between AKT and VIM, and thus enables VIM phosphorylation by AKT.

4. Discussion

It has been long known that IFN response to virus infection stimulates the expression of hundreds of ISGs, and that the antiviral effector functions of many of these ISGs jointly defend cells and the hosts against the invading viruses. Some of the antiviral ISGs include viperin[59], interferon-induced protein with tetratricopeptide repeats 1[60], PKR[61], OAS/RNase L[62], MX proteins, and others. Each of these ISGs inhibits a specific group of viruses frequently pertinent to their unique antiviral molecular mechanisms. For instance, once activated by viral double-stranded RNA, PKR causes EIF2α phosphorylation and shuts down translation to inhibit virus production. Some viruses, such as HCV and cricket paralysis virus, resist PKR-mediated inhibition by employing cap-independent translation mechanism, internal ribosomal entry site, to bypass the need for EIF2α. In addition to PKR-mediated shutdown of protein synthesis, in this study, we report a global effect of IFN treatment on protein subcellular distribution. This effect of IFN may impact many cellular functions, since the GO analysis of the affected proteins showed enrichment in multiple key cellular pathways and processes, including nucleoside phosphate metabolism, carboxylic acid metabolism, ribose phosphate metabolism, DNA metabolism, and the negative regulation of cell cycle. It is highly possible that, as a mechanism to inhibit virus infection, IFN may extend this effect to change subcellular localization of viral proteins and complexes. Importantly, depletion of MXB largely abrogates the changes in protein subcellular distribution caused by IFN, suggesting a new mechanism underlying the antiviral function of MXB.

MXB was previously reported to inhibit viruses from different virus families, including HIV-1, HBV, HCV, and HSV-1[10,44,45,63]. Distinct steps of replication of these viruses are impaired by

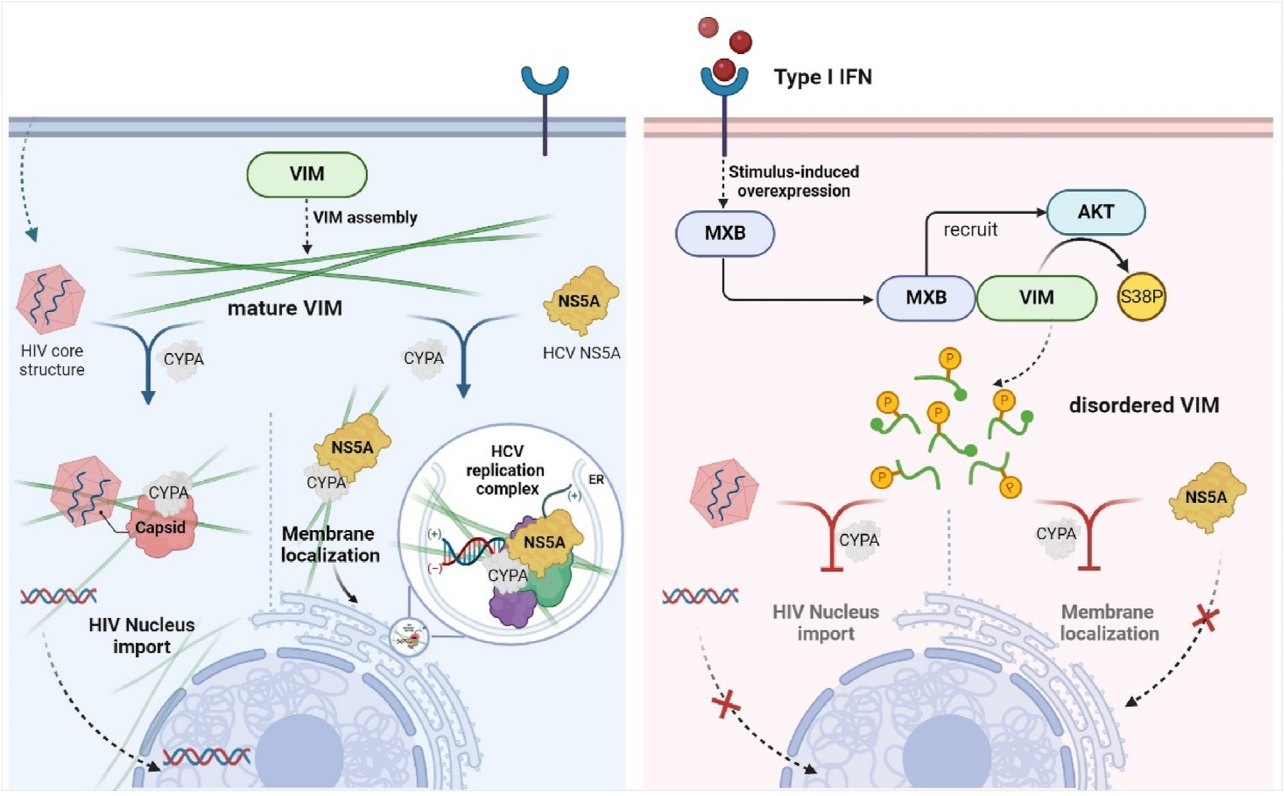

Figure 9 Model depicting MXB inhibition of HIV-1 and HCV replication by regulating the VIM network. VIM binds to HIV-1 capsid and HCV NS5A, and promotes the nuclear import of HIV-1 DNA and ER localization of HCV NS5A. When MXB is induced by IFN, MXB hijacks AKT to phosphorylate S38 in VIM, which causes a rearrangement of the VIM network, impairment of HIV-1 DNA nuclear import and HCV NS5A localization to ER, and a restriction of virus infection. The figure was created using BioRender.com.

MXB. For instance, MXB inhibits the nuclear import of HIV-1 DNA and herpesvirus DNA, disrupts ER localization of HCV NS5A protein, and reduces the production of HBV cccDNA. The specificity of MXB inhibition of each of these viruses may depend on the MXB recognition of specific viral proteins such as HIV-1 capsid. However, an equally possible scenario is that MXB may have targeted a cellular mechanism that these viruses need to hijack to replicate. The results of the present study support this model of MXB antiviral action by showing that MXB disrupts the VIM network which some viruses use to transport to the right subcellular sites to achieve efficient replication (Fig. 9). Specifically, through the interaction with both of these proteins, MXB recruits the AKT kinase to VIM and causes VIM phosphorylation at S38, which results in the VIM network reorganization and aggregation. This model of action would predict that VIM-dependent viruses, including HIV-1 and HCV, are sensitive to the MXB inhibition; said differently, the nuclear import of HIV-1 virion and ER-localization of HCV NS5A all depend on VIM (Fig. 3). In previous research, VIM was found to interact with HCV core protein[64], also with the HSV-1 capsid and tegument protein complex[65]. The link remains to be established between the dependence of HIV-1, HBV, HCV and HSV-1 on VIM and their sensitivity to MXB inhibition.

Some viruses such as IAV rely on VIM for replication, but remain insensitive to MXB restriction. In this case, VIM depletion affects endosome distribution and acidification, thus impeding the release of the IAV RNA genome from these organelles[66]. It is likely that MXB causes VIM network reorganization, but does not affect the distribution and properties of endosomes. The selective effect of MXB on VIM function may be attributed to the possibility that MXB has access to only certain populations of VIM, which partly depends on the subcellular localization of MXB. In support of this scenario, changing subcellular localization of MXB rendered the host cells resistant to IAV[67], although a role of VIM in this anti-IAV function of the modified MXB remains unclear. Alternatively, as shown in the present study and several pervious investigations, MXB-induced reorganization of VIM network may only compromise the trafficking of a subset of cargos, such as those that depend on CYPA, highlighting CYPA dependence of certain viruses on both their sensitivity to MXB and their VIM-mediated intracellular transportation[10,67,68]. One working model is that MXB preferably inhibits CYPA-dependent VIM-mediated intracellular trafficking of both cellular and viral proteins and complexes, thereby leading to the inhibition of a selective group of viruses.

Modulation of VIM structure was previously reported to involved in the early stage of HIV replication and treated as a potential therapeutic target against HIV infection[24]. VIM assembly and disassembly are regulated by phosphorylation at multiple amino acid sites, including S25, S38, S50, S55, S65, S71, S82, and S83 [56,69,70]. In this study, we observed that MXB causes VIM network reorganization by inducing S38 phosphorylation. Although multiple kinases including AKT, ERK1/2, PAK, ROCK, PKA, PKC, CAM kinase II and Aurora-B kinase were previously reported to be able to phosphorylate VIM at S38[56–58], our study showed that only AKT inhibitor or knockdown of AKT diminished MXB-induced S38 phosphorylation of VIM. Importantly, preventing the phosphorylation of VIM at S38 by either mutating

S38 to S38A or the inactivation of AKT abolished the antiviral activity of MXB, supporting the model that MXB inhibits viruses by recruiting AKT to phosphorylate VIM at S38 and impairing VIM-dependent trafficking of viral proteins and complexes. Interestingly, inhibitors of kinases PKA and ROCK also antagonize the antiviral activity of MXB, yet without affecting VIM S38 phosphorylation. This observation suggests additional phosphorylation-dependent mechanisms regulating the antiviral function of MXB. For instance, Betancor et al.[47] recently found that MXB interacts with myosin light chain phosphatase, a member of the serine/threonine protein phosphatase 1 family, which safeguards the antiviral activity of MXB by dephosphorylating the N-terminal domain of MXB. Interestingly, some phosphorylated mutants of MXB (*e.g.*, S28D/T151D or T151D/T343A) were found to extend antiviral effects to CYPA-independent HIV-1 capsid mutant, such as P90A, which was insensitive to wild type MXB[71]. Of note, while several studies reported that VIM is an interferon-inducible protein, no significant increase in VIM expression was observed upon IFN-β treatment in another previous study[72] and in our present results. One possible explanation for this discrepancy is that the response of VIM expression to IFN stimulation may vary dependent of cell-type or experimental condition, while the actual cause awaits further investigation. In this work, all the experiments on endogenous MXB utilized IFN as a stimulus, and it would be even more relevant to investigate the interaction between endogenous MXB and VIM in virus-infected cells. Unfortunately, similarly to several previous studies[43], we did not detect robust expression of endogenous MXB induced by HCV and HIV-1 infection (data not shown). Possible reasons include either the impaired ability to produce IFN in HCV-permissive Huh7.5.1 cells or virus-mediated inhibition on innate immunity activation so as to block inducing the expression of endogenous MXB by viral infection.

To date, multiple mechanisms to account for the antiviral activity of MXB have been reported, particularly in the context of restricting HIV-1 infection. One mechanism involves MXB binding to HIV-1 capsid, which leads to excessive stabilization of viral capsid and the delay of viral capsid uncoating[37]. The other mechanism is attributed to the localization of MXB to nuclear pore complex (NPC) and interaction with specific nucleoporins such as NUP214, which allows MXB to deter the docking of HIV-1 capsid to NPC and subsequent entry into the nucleus[47]. Consistently with the previous studies showing that double depletion of NUP214/TNPO1 decreases antiviral function of MXB by 2- to 3-fold[46], our data also exhibited about 2-fold inhibition of MXB antiviral activity by down-regulation of VIM, which suggests a similar importance of NUPs and IFs in inhibition of viral infection by MXB. In addition, a lower expression level of MXB tended to accumulate around nuclear envelop as reduced granule staining[39], but large cytoplasmic puncta could be observed at a higher expression level as Figs. 5A and 7G shown, which suggests more biological functions of MXB may execute in cytoplasm related with IFs. Accordingly, our study adds a new layer to the current knowledge about the mechanism underpinning the antiviral function of MXB, which may act by modulating VIM network and, as a result, interfere with viral complex trafficking and viral replication. These mechanisms may not be mutually exclusive, rather may act in concert to achieve maximal restriction of virus infections.

In summary, our study reveals a new function of MXB in regulating the organization of VIM network by recruiting AKT to phosphorylate the S38 amino acid of VIM. This function may have allowed MXB to restrict a group of different viruses that depend on VIM for intracellular trafficking and efficient replication, and thus serve as a broad antiviral effector in the context of IFN response. Accordingly, inducing expression of endogenous MXB or expressing ectopical MXB (*i.e.*, mRNA-based) may broadly suppress the infection of VIM-dependent viruses. Our results also suggest that modulating VIM network with small compounds may represent a new strategy to discover novel broad-spectrum antiviral therapies, and such host-targeting strategy was previously reported to be broad-spectrum and effective[73,74]. For instance, promoting the phosphorylation of VIM S38 by small molecules through either increasing AKT activity or specially enhancing AKT−VIM interaction may lead to a rearrangement of VIM, thereby interrupting the cellular transportation of viruses. In line with this proposal, several VIM-targeting compounds were already documented to regulate VIM structure and guard against virus infection[75,76]; yet, the exact mechanism awaits further investigation.

5. Conclusions

In this study, we reported a novel antiviral mechanism of MXB, which contributes to explaining its broad-spectrum antiviral activity. MXB hijacks AKT to phosphorylate S38 of intermediate filament VIM, which induces VIM rearrangement. This structural change of the VIM network impairs the normal intracellular transport of virus, such as nuclear import of HIV-1 DNA and ER localization of HCV NS5A, and eventually restricts viral replication in cells. These findings provide a new idea and method for universal antiviral research and corresponding drug development.

Acknowledgments

The authors appreciate the National Microbial Resource Center (No. NMRC-2020-3) and the CAMS Collection Center of Pathogenic Microorganisms (CAMS-CCPM-A) for providing valuable reagents. This work was supported by Beijing Natural Science Foundation 7242097 (to Dongrong Yi), National Natural Science Foundation of China 81902075 (to Dongrong Yi), and CAMS Innovation Fund for Medical Sciences 2021-I2M-1-038 (to Shan Cen), 2021-I2M-1-030 (to Quanjie Li), and 2021-I2M-1-043 (to Xiaoyu Li).

Author contributions

Shan Cen and Dongrong Yi designed the study; Dongrong Yi and Ni An performed the main part of the experiment; Quanjie Li conducted the bioinformatics analysis and data curation; Qian Liu, Huihan Shao and Rui Zhou performed infection assays; Jing Wang, Yongxin Zhang, Ling Ma, Xiaoyu Li, and Fei Guo contributed to the data analysis; Dongrong Yi, Ni An, and Quanjie Li prepared the original draft; Shan Cen revised the manuscript; Shan Cen and Zhenlong Liu conceived and supervised the project; all authors approved the final version of the manuscript.

Conflicts of interest

The authors declare no competing interests.

Appendix A. Supporting information

Supporting data to this article can be found online at https://doi.org/10.1016/j.apsb.2024.03.029.

References

1. Michalska A, Blaszczyk K, Wesoly J, Bluyssen HAR. A positive feedback amplifier circuit that regulates interferon (IFN)-stimulated gene expression and controls type I and type II IFN responses. *Front Immunol* 2018;**9**:1135.
2. Rojas JM, Alejo A, Martín V, Sevilla N. Viral pathogen-induced mechanisms to antagonize mammalian interferon (IFN) signaling pathway. *Cell Mol Life Sci* 2021;**78**:1423–44.
3. Ivashkiv LB, Donlin LT. Regulation of type I interferon responses. *Nat Rev Immunol* 2014;**14**:36–49.
4. Greber UF. Virus and host mechanics support membrane penetration and cell entry. *J Virol* 2016;**90**:3802–5.
5. Kumar R, Mehta D, Mishra N, Nayak D, Sunil S. Role of host-mediated post-translational modifications (PTMs) in RNA virus pathogenesis. *Int J Mol Sci* 2020;**22**:323.
6. Yi D, Li Q, Wang H, Lv K, Ma L, Wang Y, et al. Repurposing of berbamine hydrochloride to inhibit Ebola virus by targeting viral glycoprotein. *Acta Pharm Sin B* 2022;**12**:4378–89.
7. Walsh D, Naghavi MH. Exploitation of cytoskeletal networks during early viral infection. *Trends Microbiol* 2019;**27**:39–50.
8. Wu S, Du Y, Beckford J, Alachkar H. Upregulation of the EMT marker vimentin is associated with poor clinical outcome in acute myeloid leukemia. *J Transl Med* 2018;**16**:170.
9. Sodeik B. Mechanisms of viral transport in the cytoplasm. *Trends Microbiol* 2000;**8**:465–72.
10. Yi D, An N, Liu Z, Xu F, Raniga K, Li Q, et al. Human MxB inhibits the replication of hepatitis C virus. *J Virol* 2019;**93**: e01285.18.
11. Cortese M, Goellner S, Acosta EG, Neufeldt CJ, Oleksiuk O, Lampe M, et al. Ultrastructural characterization of zika virus replication factories. *Cell Rep* 2017;**18**:2113–23.
12. Suzuki Y, Craigie R. The road to chromatin—nuclear entry of retroviruses. *Nat Rev Microbiol* 2007;**5**:187–96.
13. Martin K, Helenius A. Transport of incoming influenza virus nucleocapsids into the nucleus. *J Virol* 1991;**65**:232–44.
14. Whittaker GR, Helenius A. Nuclear import and export of viruses and virus genomes. *Virology* 1998;**246**:1–23.
15. Fletcher DA, Mullins RD. Cell mechanics and the cytoskeleton. *Nature* 2010;**463**:485–92.
16. Herrmann H, Aebi U. Intermediate filaments and their associates: multi-talented structural elements specifying cytoarchitecture and cytodynamics. *Curr Opin Cell Biol* 2000;**12**:79–90.
17. Dominguez R, Holmes KC. Actin structure and function. *Annu Rev Biophys* 2011;**40**:169–86.
18. Jaworski J, Hoogenraad CC, Akhmanova A. Microtubule plus-end tracking proteins in differentiated mammalian cells. *Int J Biochem Cell Biol* 2008;**40**:619–37.
19. Fuchs E, Weber K. Intermediate filaments: structure, dynamics, function and disease. *Annu Rev Biochem* 1994;**63**:345–82.
20. Lazarides E. Intermediate filaments as mechanical integrators of cellular space. *Nature* 1980;**283**:249–55.
21. Steinert PM, Roop DR. Molecular and cellular biology of intermediate filaments. *Annu Rev Biochem* 1988;**57**:593–625.
22. Zhang Y, Wen Z, Shi X, Liu Y, Eriksson JE, Jiu Y. The diverse roles and dynamic rearrangement of vimentin during viral infection. *J Cell Sci* 2021;**134**:jcs250597.
23. Ivaska J, Pallari HM, Nevo J, Eriksson JE. Novel functions of vimentin in cell adhesion, migration, and signaling. *Exp Cell Res* 2007;**313**:2050–62.
24. Fernández Ortega C, Ramírez A, Casillas D, Paneque T, Ubieta R, Dubed M, et al. Identification of vimentin as a potential therapeutic target against HIV infection. *Viruses* 2016;**8**:98.
25. Liu S, Mok BWY, Deng S, Liu H, Wang P, Song W, et al. Mammalian cells use the autophagy process to restrict avian influenza virus replication. *Cell Rep* 2021;**35**:109213.
26. Teo CSH, Chu JJH. Cellular vimentin regulates construction of dengue virus replication complexes through interaction with NS4A protein. *J Virol* 2014;**88**:1897–913.
27. Zhang Y, Zhao S, Li Y, Feng F, Li M, Xue Y, et al. Host cytoskeletal vimentin serves as a structural organizer and an RNA-binding protein regulator to facilitate Zika viral replication. *Proc Natl Acad Sci U S A* 2022;**119**:e2113909119.
28. Haller O, Stertz S, Kochs G. The Mx GTPase family of interferon-induced antiviral proteins. *Microbes Infect* 2007;**9**:1636–43.
29. Verhelst J, Hulpiau P, Saelens X. Mx proteins: antiviral gatekeepers that restrain the uninvited. *Microbiol Mol Biol Rev* 2013; **77**:551–66.
30. Haller O, Kochs G. Human MxA protein: an interferon-induced dynamin-like GTPase with broad antiviral activity. *J Interferon Cytokine Res* 2011;**31**:79–87.
31. Haller O, Staeheli P, Schwemmle M, Kochs G. Mx GTPases: dynamin-like antiviral machines of innate immunity. *Trends Microbiol* 2015;**23**:154–63.
32. Alvarez FJ, He S, Perilla JR, Jang S, Schulten K, Engelman AN, et al. CryoEM structure of MxB reveals a novel oligomerization interface critical for HIV restriction. *Sci Adv* 2017;**3**:e1701264.
33. Fribourgh JL, Nguyen HC, Matreyek KA, Alvarez FJD, Summers BJ, Dewdney TG, et al. Structural insight into HIV-1 restriction by MxB. *Cell Host Microbe* 2014;**16**:627–38.
34. Gao S, von der Malsburg A, Paeschke S, Behlke J, Haller O, Kochs G, et al. Structural basis of oligomerization in the stalk region of dynamin-like MxA. *Nature* 2010;**465**:502–6.
35. Haller O, Kochs G. Interferon-induced mx proteins: dynamin-like GTPases with antiviral activity. *Traffic* 2002;**3**:710–7.
36. Chai K, Wang Z, Pan Q, Tan J, Qiao W, Liang C. Effect of different nuclear localization signals on the subcellular localization and anti-HIV-1 function of the MxB protein. *Front Microbiol* 2021;**12**:675201.
37. Fricke T, White TE, Schulte B, de Souza Aranha Vieira DA, Dharan A, Campbell EM, et al. MxB binds to the HIV-1 core and prevents the uncoating process of HIV-1. *Retrovirology* 2014;**11**:68.
38. Matreyek KA, Wang W, Serrao E, Singh PK, Levin HL, Engelman A. Host and viral determinants for MxB restriction of HIV-1 infection. *Retrovirology* 2014;**11**:90.
39. Goujon C, Moncorgé O, Bauby H, Doyle T, Barclay WS, Malim MH. Transfer of the amino-terminal nuclear envelope targeting domain of human MX2 converts MX1 into an HIV-1 resistance factor. *J Virol* 2014;**88**:9017–26.
40. Buffone C, Schulte B, Opp S, Diaz-Griffero F. Contribution of MxB oligomerization to HIV-1 capsid binding and restriction. *J Virol* 2015; **89**:3285–94.
41. Kochs G, Haller O. Interferon-induced human MxA GTPase blocks nuclear import of Thogoto virus nucleocapsids. *Proc Natl Acad Sci U S A* 1999;**96**:2082–6.
42. Kochs G, Haller O. GTP-bound human MxA protein interacts with the nucleocapsids of Thogoto virus (Orthomyxoviridae). *J Biol Chem* 1999;**274**:4370–6.
43. Goujon C, Moncorgé O, Bauby H, Doyle T, Ward CC, Schaller T, et al. Human MX2 is an interferon-induced post-entry inhibitor of HIV-1 infection. *Nature* 2013;**502**:559–62.
44. Liu Z, Pan Q, Ding S, Qian J, Xu F, Zhou J, et al. The interferon-inducible MxB protein inhibits HIV-1 infection. *Cell Host Microbe* 2013;**14**:398–410.
45. Crameri M, Bauer M, Caduff N, Walker R, Steiner F, Franzoso FD, et al. MxB is an interferon-induced restriction factor of human herpesviruses. *Nat Commun* 2018;**9**:1980.
46. Dicks MD, Betancor G, Jimenez Guardeño JM, Pessel Vivares L, Apolonia L, Goujon C, et al. Multiple components of the nuclear pore complex interact with the amino-terminus of MX2 to facilitate HIV-1 restriction. *PLoS Pathog* 2018;**14**:e1007408.
47. Betancor G, Jimenez Guardeño JM, Lynham S, Antrobus R, Khan H, Sobala A, et al. MX2-mediated innate immunity against HIV-1 is

regulated by serine phosphorylation. *Nat Microbiol* 2021;**6**:1031−42.
48. Zhang Y, Wen Z, Shi X, Liu YJ, Eriksson JE, Jiu Y. The diverse roles and dynamic rearrangement of vimentin during viral infection. *J Cell Sci* 2020;**134**:jcs250597.
49. Ramos I, Stamatakis K, Oeste CL, Pérez-Sala D. Vimentin as a multifaceted player and potential therapeutic target in viral infections. *Int J Mol Sci* 2020;**21**:4675.
50. Xie L, Chen L, Zhong C, Yu T, Ju Z, Wang M, et al. MxB impedes the NUP358-mediated HIV-1 pre-integration complex nuclear import and viral replication cooperatively with CPSF6. *Retrovirology* 2020;**17**:16.
51. Kane M, Rebensburg SV, Takata MA, Zang TM, Yamashita M, Kvaratskhelia M, et al. Nuclear pore heterogeneity influences HIV-1 infection and the antiviral activity of MX2. *Elife* 2018;**7**:e35738.
52. Li Y, Kar AK, Sodroski J. Target cell type-dependent modulation of human immunodeficiency virus type 1 capsid disassembly by cyclophilin A. *J Virol* 2009;**83**:10951−62.
53. Yang F, Robotham JM, Grise H, Frausto S, Madan V, Zayas M, et al. A major determinant of cyclophilin dependence and cyclosporine susceptibility of hepatitis C virus identified by a genetic approach. *PLoS Pathog* 2010;**6**:e1001118.
54. Bouamrani A, Ramus C, Gay E, Pelletier L, Cubizolles M, Brugière S, et al. Increased phosphorylation of vimentin in noninfiltrative meningiomas. *PLoS One* 2010;**5**:e9238.
55. Snider NT, Omary MB. Post-translational modifications of intermediate filament proteins: mechanisms and functions. *Nat Rev Mol Cell Biol* 2014;**15**:163−77.
56. Dave JM, Bayless KJ. Vimentin as an integral regulator of cell adhesion and endothelial sprouting. *Microcirculation* 2014;**21**:333−44.
57. Bargagna Mohan P, Lei L, Thompson A, Shaw C, Kasahara K, Inagaki M, et al. Vimentin phosphorylation underlies myofibroblast sensitivity to withaferin A *in vitro* and during corneal fibrosis. *PLoS One* 2015;**10**:e0133399.
58. Romano R, Calcagnile M, Margiotta A, Franci L, Chiariello M, Alifano P, et al. RAB7A regulates vimentin phosphorylation through AKT and PAK. *Cancers* 2021;**13**:2220.
59. Gizzi AS, Grove TL, Arnold JJ, Jose J, Jangra RK, Garforth SJ, et al. A naturally occurring antiviral ribonucleotide encoded by the human genome. *Nature* 2018;**558**:610−4.
60. Daffis S, Szretter KJ, Schriewer J, Li J, Youn S, Errett J, et al. 2′-*O* Methylation of the viral mRNA cap evades host restriction by IFIT family members. *Nature* 2010;**468**:452−6.
61. Pfaller CK, Li Z, George CX, Samuel CE. Protein kinase PKR and RNA adenosine deaminase ADAR1: new roles for old players as modulators of the interferon response. *Curr Opin Immunol* 2011;**23**:573−82.
62. Hornung V, Hartmann R, Ablasser A, Hopfner KP. OAS proteins and cGAS: unifying concepts in sensing and responding to cytosolic nucleic acids. *Nat Rev Immunol* 2014;**14**:521−8.
63. Wang Y, Niklasch M, Liu T, Wang Y, Shi B, Yuan W, et al. Interferon-inducible MX2 is a host restriction factor of hepatitis B virus replication. *J Hepatol* 2020;**72**:865−76.
64. Ghosh S, Ahrens WA, Phatak SU, Hwang S, Schrum LW, Bonkovsky HL. Association of filamin A and vimentin with hepatitis C virus proteins in infected human hepatocytes. *J Viral Hepat* 2011;**18**:e568−77.
65. Scholtes LD, Yang K, Li LX, Baines JD. The capsid protein encoded by U_L17 of herpes simplex virus 1 interacts with tegument protein VP13/14. *J Virol* 2010;**84**:7642−50.
66. Wu W, Panté N. Vimentin plays a role in the release of the influenza A viral genome from endosomes. *Virology* 2016;**497**:41−52.
67. Steiner F, Pavlovic J. Subcellular localization of MxB determines its antiviral potential against influenza A virus. *J Virol* 2020;**94**:e00125.20.
68. Sultana T, Mamede JI, Saito A, Ode H, Nohata K, Cohen R, et al. Multiple pathways to avoid beta interferon sensitivity of HIV-1 by mutations in capsid. *J Virol* 2019;**93**:e00986.19.
69. Eriksson JE, He T, Trejo Skalli AV, Härmälä Braskén AS, Hellman J, Chou YH, et al. Specific *in vivo* phosphorylation sites determine the assembly dynamics of vimentin intermediate filaments. *J Cell Sci* 2004;**117**:919−32.
70. Evans RM. Phosphorylation of vimentin in mitotically selected cells. *In vitro* cyclic AMP-independent kinase and calcium-stimulated phosphatase activities. *J Cell Biol* 1989;**108**:67−78.
71. Betancor G, Bangham M, Jeon JK, Shah K, Lynham S, Jimenez Guardeño JM, et al. MX2 viral substrate breadth and inhibitory activity are regulated by protein phosphorylation. *mBio* 2022;**13**:e01714.22.
72. Ignarro RS, Bombeiro AL, Chiarotto GB, Cartarozzi LP, Coser LO, Ghizoni E, et al. Interferon-β induces major histocompatibility complex of class I (MHC-I) expression and a proinflammatory phenotype in cultivated human astrocytes. *Differentiation* 2022;**128**:43−56.
73. Wu KX, Yogarajah T, Loe MWC, Kaur P, Lee RCH, Mok CK, et al. The host-targeting compound peruvoside has a broad-spectrum antiviral activity against positive-sense RNA viruses. *Acta Pharm Sin B* 2023;**13**:2039−55.
74. Aliyari SR, Ghaffari AA, Pernet O, Parvatiyar K, Wang Y, Gerami H, et al. Suppressing fatty acid synthase by type I interferon and chemical inhibitors as a broad spectrum anti-viral strategy against SARS-CoV-2. *Acta Pharm Sin B* 2022;**12**:1624−35.
75. Li Z, Wu J, Zhou J, Yuan B, Chen J, Wu W, et al. A vimentin-targeting oral compound with host-directed antiviral and anti-inflammatory actions addresses multiple features of COVID-19 and related diseases. *mBio* 2021;**12**:e0254221.
76. Li Z, Paulin D, Lacolley P, Coletti D, Agbulut O. Vimentin as a target for the treatment of COVID-19. *BMJ Open Respir Res* 2020;**7**:e000623.